Balitsky–Kovchegov equation

Heikki Mäntysaari

Pro Gradu
University of Jyväskylä
Department of Physics
Supervisor: Dr. Tuomas Lappi
November 2011

Abstract

In high-energy particle physics the energy evolution of various quantities can be calculated from the Balitsky-Kovchegov (BK) equation. Depending on the frame that is used to describe the process, the BK equation can be seen to describe either the energy evolution of the virtual photon wave function or the gluon distribution function of a hadron.

In this work the BK equation is derived at leading logarithm accuracy from QCD and solved analytically in some special cases. In order to derive it the quantum field theory on the light cone is introduced. Part of the higher order corrections to the BK equation, namely the running strong coupling constant and the kinematical constraint effects, are studied numerically.

As a result it is shown that the running coupling slows down the evolution significantly compared with the evolution obtained with a fixed coupling constant. The different running coupling prescriptions used in the literature also cause significantly different evolution speeds. In addition the running coupling changes the asymptotical shape of the solution. On the other hand the kinematical constraint effects are shown to affect mainly the evolution speed while leaving the shape of the solution intact.

The numerical codes developed in this work can be used when studying the phenomenology of high-energy QCD.

Tiivistelmä

Hiukkasfysiikassa monien suureiden energiariippuvuus suurienergisissä prosesseissa voidaan laskea Balitsky–Kovchegov (BK) -yhtälöstä. Sirontaprosessin kuvaamiseen käytetystä koordinaatistosta riippuen BK-yhtälön voidaan tulkita kuvaavan joko virtuaalisen fotonin aaltofunktion tai hadronin gluonijakaumafunktion energiariippuvutta.

Tässä työssä BK-yhtälö johdetaan johtavaan kertalukuun QCD:stä ja ratkaistaan analyyttisesti muutamassa erikoistapauksessa. BK-yhtälön johtamiseksi esitellään kvanttikenttäteoria valokartiokoordinaatistossa. Korkeamman kertaluvun korjauksia BK-yhtälöön tutkitaan ratkaisemalla BK-yhtälö numeerisesti käyttäen juoksevaa vahvan vuorovaikutuksen kytkinvakiota ja kinemaattista rajoitetta.

Tutkimuksen tuloksena havaitaan, että juokseva kytkinvakio hidastaa energiaevoluutiota selvästi verrattuna tapaukseen, jossa vahvan vuorovaikutuksen kytkinvakio ei riipu skaalasta. Lisäksi huomataan, että kirjallisuudessa esiintyvät toisistaan eroavat tavat lisätä juokseva kytkinvakio BK-yhtälöön johtavat selvästi toisistaan eroaviin evoluutionopeuksiin. Juokseva kytkinvakio myös muuttaa ratkaisun asymptoottista muotoa verrattuna tapaukseen, jossa kytkinvakio ei riipu skaalasta. Toisaalta kinemaattinen ehto vaikuttaa pääasiassa vain evoluutionopeuteen, mutta jättää ratkaisun muodon samaksi.

Tässä työssä kehitettyjä numeerisia ohjelmia voidaan käyttää jatkossa tutkittaessa QCD-prosesseja suurella energialla.

Contents

Chapter 1

Introduction

In particle physics the elementary matter particles and their interactions, excluding gravity, are described by the Standard Model. It describes three kinds of interactions: electromagnetic, weak and strong. Moreover, electromagnetic and weak interactions are described as two aspects of the same force, namely the electroweak interaction. All matter particles interact via the electroweak interaction. The third interaction in the Standard Model is the strong interaction described by quantum chromodynamics (QCD). Quarks and gluons, the particles that e.g. a proton consists of, also interact via the strong interaction.

The Standard Model is known to be an accurate description of all measured collider physics phenomena, but there are still a few open questions. In the electroweak sector the existence of the Higgs boson, predicted by the Standard Model, is under intensive experimental research. In addition, measured neutrino oscillations suggest that neutrinos have nonzero mass, in contradiction to the Standard Model. In quantum chromodynamics the properties of the quark-gluon plasma (QGP), the state of matter that can be produced in ultrarelativistic heavy ion collisions, are not known in detail.

Experimental results show that the gluon density inside the proton (and similarly inside the nucleus) grows rapidly when the fraction of proton momentum carried by the gluon, the Bjorken x, decreases. This is equivalent to probing the hadron at high energy, and allows us to consider a proton or a nucleus as a medium of dense gluon matter known as the Color Glass Condensate (CGC). For a review of the CGC framework, see for example Refs. [1, 2]. The energy dependence of observables in this regime can be calculated through evolution equations which are derived from QCD in the high energy limit. One of these evolution equations is known as the Balitsky-Kovchegov (BK) equation, which is the topic of this Thesis.

The Color Glass Condensate can also be used to describe the QCD dynam-

ics of the earliest stages of the ultrarelativistic heavy ion collisions studied experimentally at RHIC and LHC. Theoretically the spacetime evolution of the QGP produced in these collisions is well understood in terms of relativistic hydrodynamics which requires information about the initial condition. It should be possible to calculate the initial condition from the CGC framework, as both of the colliding nuclei can be described as a dense gluon matter, see for example Ref. [3] and references therein.

This work is structured as follows. In Chapter 2 we discuss QCD at high energy in general. In Chapter 3 we introduce light cone quantum field theory, which we use to derive the Balitsky-Kovchegov equation in Chapter 4. After studying its properties analytically and discussing the higher order corrections, we study it numerically in Chapter 5.

Notation

Vectors are written as a plain letters without any vector sign, e.g. p for the 4-momentum. Whenever it is clear in the context, we denote the length of the two-dimensional transverse vectors as $r = |\bar{r}|$. The system of units known as the natural units, in which $\hbar = c = k_{\mathrm{B}} = 1$, is used. In this case the fine structure constant is $\alpha_{\mathrm{em}} = e^2/(4\pi) \approx 137^{-1}$, and

$$[\text{mass}] = [\text{energy}] = [\text{time}]^{-1} = [\text{length}]^{-1} = \text{GeV}. \tag{1.1}$$

The relation between gigaelectronvolts (GeV) and femtometers is

$$1 \text{ GeV} = 5.0677 \text{ fm}^{-1}. \tag{1.2}$$

Chapter 2

High energy scattering in QCD

2.1 Deep inelastic scattering

Deep inelastic scattering (DIS) is a powerful way to measure the internal structure of hadrons and to test perturbative QCD. For example, one can extract the parton distribution functions from the measured total lepton-hadron cross section. In DIS a lepton scatters off a hadron which then breaks up into other particles making the process inelastic. Let us consider deep inelastic scattering of the lepton l off the nucleus N. In this case we can write the process as

$$l(\ell) + N(P) \to l'(\ell') + X(P_X), \tag{2.1}$$

where P is the momentum of the incoming nucleus and ℓ and ℓ' are the momenta of the incoming and outgoing lepton, respectively. In this process the nucleus breaks up and forms many different particles, which are denoted by X, with momentum P_X. The situation is shown schematically in Fig. 2.1.

As leptons are simple, pointlike particles, photon emission from a lepton is well understood in terms of quantum electrodynamics. On the other hand the photon-proton (or photon-nucleus) scattering is more difficult to formulate, as the proton is not a simple object but contains valence quarks, sea quarks

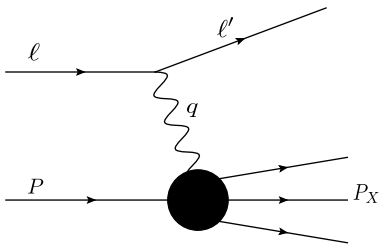

Figure 2.1. Deep inealstic scattering.

formed by the quark-antiquark fluctuations, and gluons. The role of the lepton in these experiments is to act as a source of virtual photons, and the interesting physics is encoded in the virtual photon-hadron scattering. Notice that when we discuss the parton constituents of the hadron, we are working in the infinite momentum frame where the hadron has a large momentum. This parton picture is not valid in the frame where the proton momentum is small, as we will discuss in Sec. 2.3.

To describe the kinematics of nuclear deep inelastic scattering we define the following Lorentz invariant variables:

$$s = (P+q)^2 \tag{2.2}$$

$$q^2 \equiv -Q^2 \equiv (\ell - \ell')^2 \tag{2.3}$$

$$\nu \equiv \frac{P\cdot q}{m_A} = \frac{W^2+Q^2-m_A^2}{2m_A} \tag{2.4}$$

$$x \equiv \frac{AQ^2}{2P\cdot q} = \frac{AQ^2}{2m_A\nu} = \frac{AQ^2}{Q^2+W^2-m_A^2}. \tag{2.5}$$

If the target hadron is a proton, we set the mass number of the nucleus, A, to one. Here s is the Mandelstam variable describing the total energy in the center of mass (CMS) frame, $W^2 = (P+q)^2$ is the CMS energy for the photon-nucleus scattering, m_A is the mass of the nucleus and Q^2 is the virtuality of the photon. The interpretation of ν is that it gives the total energy transferred in the process in the target rest frame: $\nu = E_l - E_l'$ where E_l and E_l' are the lepton energies at the beginning and at the end of the process in the proton rest frame, respectively.

The variable x is called Bjorken x and its interpretation in the infinite momentum frame is that it gives the fraction of the hadron momentum carried by the quark or the gluon taking part in the scattering process. Notice that in order to get a small x the momentum of the proton or the photon must be large.

2.2 Energy evolution and saturation scale

Let us first consider a DIS of a lepton off the proton in the infinite momentum frame. Due to the uncertainty relation the virtuality of the photon, Q^2, sets the scale r of the objects that the photon can see: $r \sim 1/Q$. That is, the apparent size of the partons seen by the photon is $1/Q^2$. If Q^2 is large enough, the target appears to be a dilute system of quarks and gluons.

The parton distribution function, denoted by $f_i(x, Q^2)$, has, in the lowest order, an interpretation as a probability to find a parton i (quark, antiquark or

gluon) with momentum fraction x by using a probing photon whose virtuality is Q^2. We are here interested in the high energy limit, which corresponds to small x, as $s \sim Q^2/x$. In this region the proton constituents are mainly gluons, hence from now on we neglect all quarks. In terms of parton distribution functions, $f_g(x, Q^2)$ grows rapidly as x decreases, and the quark distributions can be neglected. Notice that when energy increases and Q^2 is kept fixed, smaller and smaller values of x are probed, and thus we can talk about energy evolution.

The physical interpretation of this evolution is that at small x (when we can neglect everything but gluons) we see more and more soft gluons, emitted by harder gluons. By soft gluons we mean gluons which carry a small fraction x of the proton momentum, $x \ll 1$. The apparent size of the gluon is $\sim 1/Q^2$ as, according to the uncetainty principle, the characteristic length scale is $\sim 1/Q$. Thus, if Q^2 is large enough, there is a lot of phase space available for new soft gluons and we can expect that the number of gluons increases with decreasing x. The situation is shown schematically in Fig. 2.2.

Now if we keep Q^2 fixed and move to smaller values of x, or alternatively keep x fixed (and small) and decrease Q^2, we see that at some point gluons start to overlap and, due to the self-coupling of gluons in QCD, we have to take into account gluon recombination processes. The larger the size of the gluons, the earlier they fill the available area and start to recombine. When this state is reached, decreasing x further will not increase the gluon density significantly. At fixed x we can define the saturation scale Q_s as the momentum scale at which the nonlinear effects (gluon recombination) become important. The characteristic length scale is then $\sim 1/Q_s$. We shall give more exact definition for Q_s in our framework later in Sec. 5.2.

The energy (or scale) evolution of these parton distribution functions can be considered at different limits of QCD. At sufficiently large scale $Q^2 \gg \Lambda^2_{\mathrm{QCD}}$, the Q^2 evolutions can be derived from the perturbative QCD. The result is known as the DGLAP (Dokshitzer–Gribov–Lipatov–Altarelli–Parisi) equation which was first derived in Refs. [4–6]. On the other hand at small x (high energy) limit the evolution in x is described by an another evolution equation known as the Balitsky–Kovchegov (BK) equation. In this work we study the BK equation in detail.

2.3 Dipole picture

In the previous sections we worked in the infinite momentum frame where a virtual photon scattered off the proton which is described as a system of quarks and gluons. All the QCD evolution took place inside the proton, and

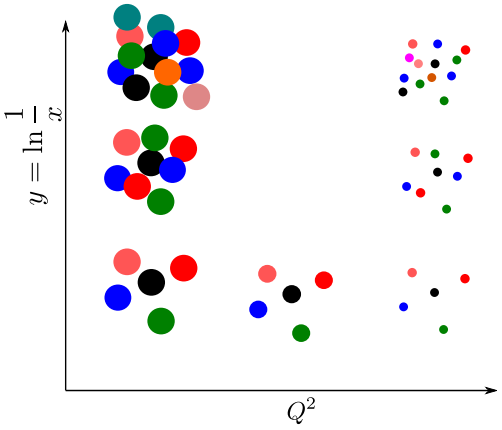

Figure 2.2. Gluons in y, Q^2 plane. As rapidity y increases, the number of gluons with apparent size $1/Q^2$ increases.

the parton distributions of the proton evolve as a function of virtuality Q^2 and Bjorken x.

On the other hand we can view the same virtual photon-proton scattering in a frame in which the proton momentum is small. In this frame the deep inelastic electron-proton scattering is described as follows: first an incoming electron emits a virtual photon γ^*, which then fluctuates into a quark-antiquark ($q\bar{q}$) color dipole. This dipole then scatters elastically off the proton and recombines to form the final state particles, e.g. a photon γ or a meson V. This process is shown schematically in Fig. 2.3, where we denote by z the fraction of virtual photon momentum carried by the quark.

This picture, known as the dipole model, is valid at small x, where one can show that the lifetime of such a quantum fluctuation which produces the $q\bar{q}$ pair is much larger than the typical timescale of the interaction [7]. In this section we discuss the total $\gamma^* p$ cross section and how to calculate it in the dipole model. A more complete discussion can be found from Ref. [8] where the dipole model is used to describe the HERA DIS data.

Let us study virtual photon-proton scattering. Following Ref. [8] the total $\gamma^* p$ cross section can be written as

$$\sigma_{T,L}^{\gamma^* p} = \sum_f \int \mathrm{d}^2 r_T \int_0^1 \mathrm{d}z [\Psi^* \Psi]_{T,L}^f (z, Q^2) \sigma_{q\bar{q}}(x, r_T), \tag{2.6}$$

where T and L refer to transverse and longitudinal polarization states of the virtual photon and f is the flavor of the quark. The virtual photon wave function squared, $\Psi^*\Psi$, will be derived later in Sec. 3.2, and its interpretation

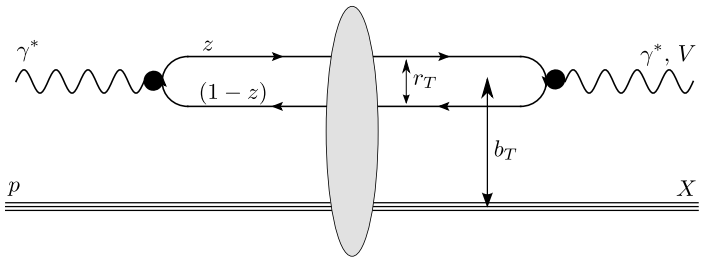

Figure 2.3. Dipole-proton scattering.

is that Ψ gives the probability amplitude for γ^* to fluctuate into the $q\bar{q}$ dipole, and Ψ^* is the probability amplitude for $q\bar{q}$ to form a virtual photon.

The dipole-proton cross section $\sigma_{q\bar{q}}(x, r_T)$ can be obtained from the elastic dipole-proton scattering amplitude $\mathcal{A}(x, r_T, \Delta)$ using the optical theorem [7, 9]:

$$\sigma_{q\bar{q}} = 2\,\mathrm{Im}\,\mathcal{A}(x, r_T, \Delta = 0) = 2\int \mathrm{d}^2 b_T N(x, r_T, b_T) = \sigma_0 N(x, r_T). \qquad (2.7)$$

Here $N(x, r_T, b_T)$ is the imaginary part of the forward elastic dipole-proton scattering amplitude. To get the last equality we neglected the impact parameter dependence and assumed that the b_T integral gives only a constant factor $\sigma_0/2$ which we treat as a fit parameter. We will get the scattering amplitude $N(x, r_T)$ later in Chapter 4 by solving the Balitsky-Kovchegov (BK) equation.

The assumption that the impact parameter can be neglected corresponds to the scattering off an infinitely large uniform nucleus. This approximation is justified as one can obtain a good description of the current HERA data with this approximation as we will discuss in Sec. 4.5, and we shall neglect the impact parameter dependence throughout this work. We will discuss shortly the impact parameter dependent BK equation in Sec. 4.7.

Notice that in this formalism the flux factor is included in the definition of the scattering amplitude, and N is a dimensionless quantity. Its interpretation is nothing but the probability for the $q\bar{q}$ dipole to scatter off the proton. In this context the unitarity limit $N \leq 1$ following from the requirement that the S matrix is unitary is easy to understand. We expect that $N \to 1$ at small x, which can be interpreted as a limit when the gluon density in the target is large, see discussion in the previous section. In addition the limit $N \to 1$ when r_T is large is expected. On the other hand N should go to zero in the limit $r_T \to 0$, as in that limit the dipole would appear as color neutral.

Once the $\gamma^* p$ cross section, Eq. (2.6), is known, we can directly calculate

the proton structure function F_2 [7]:

$$F_2(x,Q^2) = \frac{Q^2}{4\pi^2\alpha_{\mathrm{em}}}(\sigma_T^{\gamma^* p} + \sigma_L^{\gamma^* p}). \tag{2.8}$$

Similarly the longitudinal structure function F_L reads

$$F_L(x,Q^2) = \frac{Q^2}{4\pi^2\alpha_{\mathrm{em}}}\sigma_L^{\gamma^* p}. \tag{2.9}$$

The structure functions are physical observables which are measured experimentally in deep inelastic electron-proton scattering and without (referring to the dipole model) [10]. We will compute F_2 later in Sec. 5.6 and compare it with the experimental data in order to test the validity of our results.

Chapter 3

Quantum field theory on the light cone

3.1 Introduction

The laws of physics should not depend on the parametrization of the spacetime: one can calculate the Lorentz invariant observables in any frame of reference and obtain the same results. A familiar way to parametrize the spacetime and develop the quantum field theory (QFT) is sometimes called *instant form*, where we know the system at initial time everywhere on the hypersurface $t = 0$ (or $t = -\infty$). When the initial state is known, the system can (in principle) be propagated to a later time t using the equations of motion.

A straightforward way to move between the parametrizations is to apply Lorentz transformations. The special theory of relativity then assures that the laws of physics, and Lorentz-invariant quantities such as the cross sections, do not change. However, not all the parametrizations are reachable by means of Lorentz transformations, because we cannot boost to a frame moving at exactly velocity $v = 1$. The quantum field theory in this frame of reference is known as the light-cone quantum field theory (LCQFT). It has a few advantages compared with the traditional QFT in the instant form: interacting theory and free theory vacuums are the same and the hadronic wave functions can be computed as an expansion of Fock states [11].

A complete discussion of the LCQFT goes beyond the scope of this work. In this Chapter we shall only quote the most important results which are needed in order to derive the Balitsky-Kovchegov equation. A more detailed review can be found e.g. from Ref. [11], which we follow closely in the following discussion.

Let us denote a normal (instant form) 4-vector by $x = (x^0, x^1, x^2, x^3)$,

where x^0 is the time component and x^i ($i \geq 1$) are the spatial components. The metric tensor is the familiar one

$$g_{\mu\nu} = \begin{pmatrix} 1 & 0 & 0 & 0 \\ 0 & -1 & 0 & 0 \\ 0 & 0 & -1 & 0 \\ 0 & 0 & 0 & -1 \end{pmatrix}. \tag{3.1}$$

The light-cone coordinates are defined as $x^+ = \frac{1}{\sqrt{2}}(x^0 + x^3)$ and $x^- = \frac{1}{\sqrt{2}}(x^0 - x^3)$, and a 4-vector reads $x = (x^+, x_T, x^-)$, where $x_T = (x^1, x^2)$. The transverse components of the vector are the same in both coordinate systems, and the x^+ component is called light-cone time. Now the spatial 3-vector is $\bar{x} = (x^-, x_T)$. The metric tensor in tihs basis reads

$$g_{\mu\nu} = \begin{pmatrix} 0 & 0 & 0 & 1 \\ 0 & -1 & 0 & 0 \\ 0 & 0 & -1 & 0 \\ 1 & 0 & 0 & 0 \end{pmatrix}, \tag{3.2}$$

and the inner products become $x \cdot y = x^+ y^- + x^- y^+ - x_T \cdot y_T$. For a 4-momentum vector $p = (p^+, p_T, p^-)$, where now p^- represents the light-cone energy (as it conjugates with the light-cone time x^+), the on-shell condition reads

$$p^2 = m^2 \Rightarrow p^- = \frac{p_T^2 + m^2}{2p^+}. \tag{3.3}$$

This relation is simpler than the corresponding condition in the instant form coordinates, $E = \sqrt{\vec{p}^2 + m^2}$, as Eq. (3.3) does not have the square root but it is linear in p_T^2 and m^2.

A scalar field theory can be now quantized on the light cone by writing the field $\phi(x)$ in terms of creation and annihilation operators $\tilde{a}^\dagger$ and $\tilde{a}$ as

$$\phi(x) = \int \frac{\mathrm{d}^3\bar{p}}{\sqrt{(2\pi)^3}\sqrt{2p^+}} [e^{ip\cdot x}\tilde{a}^\dagger(\bar{p}) + e^{-ip\cdot x}\tilde{a}(\bar{p})]. \tag{3.4}$$

The vector $\bar{p}$ is the spatial part of the light-cone momentum, $\bar{p} = (p^+, p_T)$. Here we have included a factor $(2p^+)^{-1/2}$ in the integration measure following the convention used e.g. in Ref. [11]. The operators $\tilde{a}^\dagger$ and $\tilde{a}$ are assumed to obey a commutation relation

$$[\tilde{a}(\bar{p}), \tilde{a}^\dagger(\bar{q})] = \delta^3(\bar{p} - \bar{q}). \tag{3.5}$$

Similarly for a fermion field ψ we write

$$\psi(x) = \sum_s \int \frac{\mathrm{d}^3\bar{p}}{\sqrt{(2\pi)^3}\sqrt{2p^+}} \left[e^{-ip\cdot x} b_s(\bar{p}) u_s(p) + e^{ip\cdot x} d_s^\dagger(\bar{p}) v_s(p)\right]. \tag{3.6}$$

Here $b_s(\bar{p})$ destroys a fermion and $d_s^\dagger(\bar{p})$ creates an antifermion with spin s and momentum p, and u and v are the spinors for a spin-1/2 fermion and an antifermion, respectively. Fermionic operators are assumed to satisfy an anticommutation relation

$$\{b_s(\bar{p}), b_{s'}^\dagger(\bar{q})\} = \delta^3(\bar{p} - \bar{q})\delta_{ss'}, \tag{3.7}$$

and similarly for d. Finally, the gauge field A can be written as

$$A_\mu(x) = \sum_\lambda \int \frac{\mathrm{d}^3\bar{p}}{\sqrt{(2\pi)^3 2p^+}} \left[e^{-ip\cdot x} a^\lambda(\bar{p})\varepsilon_\mu^\lambda(p) + e^{ip\cdot x} a^{\lambda\,\dagger}(\bar{p})\varepsilon_\mu^{*\lambda}(p)\right], \tag{3.8}$$

where λ is the polarization of the field and ε is the polarization vector. The operators $a^{\lambda\,\dagger}$ and $a^{\lambda'}$ satisfy the same commutation relation as the scalar field operators $\tilde{a}^\dagger$ and $\tilde{a}$, Eq. (3.5), with an additional factor $\delta_{\lambda\lambda'}$.

We will also need the interaction part of the light-cone QED Hamiltonian, which reads (recall that P^- is the light-cone energy) [11]

$$\begin{aligned} P_{\mathrm{int}}^- &= e \int \mathrm{d}^3\bar{x}\, \bar{\psi} \not{A} \psi \\ &\quad + e^2 \int \mathrm{d}^3\bar{x} \left[\bar{\psi}\gamma^+\psi \frac{1}{(i\partial_-)^2} \bar{\psi}\gamma^+\psi + \bar{\psi}\not{A}\frac{\gamma^+}{i\partial_-}\not{A}\psi\right]. \end{aligned} \tag{3.9}$$

Here we use the notation $\not{A} = A_\mu\gamma^\mu$. The last two terms describe interactions like $ff\bar{f}\bar{f}$ and $\gamma\gamma f\bar{f}$ (where f stands for a fermion and $\bar{f}$ for an antifermion, and γ is a photon) which are not present in the instant form QED. In this work we do not have to deal with these complicated interactions, because when we calculate the $\gamma^* \to q\bar{q}$ (virtual photon to quark-antiquark pair) splitting in the next section, we only need the first term which is similar as in the instant form.

3.2 Virtual photon wave function

In Sec. 2.3 we noticed that in the dipole picture deep inelastic scattering can be factorized into several steps. First an incoming virtual photon fluctuates into the quark-antiquark dipole. This dipole then scatters off the target and finally forms some final state particles.

The probability for a virtual photon to fluctuate into the quark-antiquark ($q\bar{q}$) dipole can be calculated in terms of light cone perturbation theory. We could use directly the Feynman rules of the LCQFT to write down the amplitude for the $\gamma^* \to q\bar{q}$ splitting, but in this section we shall compute it

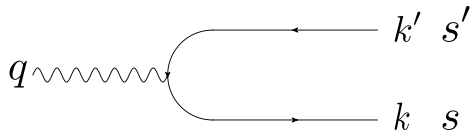

Figure 3.1. Virtual photon fluctuates to the quark-antiquark dipole. The momentum and the spin of the quark (antiquark) are k (k') and s (s'), respectively.

in a more transparent way. We quote the Feynman rules of the light-cone perturbation theory and use them to calculate the amplitude for the gluon emission process ($q \to qg$) in Sec. 3.3.

First we define a virtual photon state with momentum $\bar{q}$ and polarization λ in the free (non-interacting) theory to be

$$|\gamma^*(\bar{q})\rangle_0 = a^\lambda(\bar{q})|0\rangle. \tag{3.10}$$

If we denote the Hamiltonian of the free theory by P_0^-, we have

$$P_0^-|\gamma^*\rangle_0 = q^-|\gamma^*\rangle_0. \tag{3.11}$$

Similarly we can write the $q\bar{q}$ dipole state in this theory as

$$|q_s(\bar{k})\bar{q}_{s'}(\bar{k}')\rangle_0 = b_s^\dagger(\bar{k})d_{s'}^\dagger(\bar{k}')|0\rangle \tag{3.12}$$

from which it follows that

$$P_0^-|q_s(\bar{k})\bar{q}_{s'}(\bar{k}')\rangle_0 = (k^- + k'^-)|q_s(\bar{k})\bar{q}_{s'}(\bar{k}')\rangle_0. \tag{3.13}$$

Here k, k', s and s' are the momenta and the spin of the quark and the antiquark, respectively. The situation is shown schematically in Fig. 3.1.

We shall then use perturbation theory similarly as in quantum mechanics. We assume that the virtual photon state in the interacting theory, $|\gamma^*\rangle$, can be written as the free theory state $|\gamma^*\rangle_0$ plus a small perturbation

$$|\gamma^*\rangle = |\gamma^*\rangle_0 + \sum_{ss'}\int \mathrm{d}^3\bar{l}\,\mathrm{d}^3\bar{l}'\delta^3(\bar{q}-\bar{l}-\bar{l}')\psi_{ss'}(\bar{l})|q_s(\bar{l})\bar{q}_{s'}(\bar{l}')\rangle_0 + \mathcal{O}(e^2) \tag{3.14}$$

where the yet unknown function $\psi_{ss'}$ is called the virtual photon wave function. As the splitting $\gamma^* \to q\bar{q}$ includes one coupling between a fermion line and a gauge field, we expect that $\psi_{ss'} \sim e$, and thus we can neglect terms which are higher order in electromagnetic coupling α_{em}, or equivalently, elementary charge e (recall that $\alpha_{\mathrm{em}} = e^2/(4\pi)$).

We can then close Eq. (3.14) by ${}_0\langle q_{\hat{s}}(\bar{k})q_{\hat{s}'}(\bar{k}')|$ and use the orthogonality of the non-interacting states,

$${}_0\langle q_{\hat{s}}(\bar{k})q_{\hat{s}'}(\bar{k}')|q_s(\bar{l})q_{s'}(\bar{l}')\rangle_0 = \delta^3(\bar{k}-\bar{l})\delta^3(\bar{k}'-\bar{l}')\delta_{s\hat{s}}\delta_{s'\hat{s}'}. \tag{3.15}$$

to get

$$ {}_0\langle q_{\hat{s}}(\bar{k}) q_{\hat{s}'}(\bar{k}')|\gamma^*\rangle_0 = 0 + \delta^3(\bar{q}-\bar{k}-\bar{k}')\psi_{\hat{s}\hat{s}'}(\bar{k}). \tag{3.16} $$

On the other hand we can close Eq. (3.14) by ${}_0\langle q_{\hat{s}}(\bar{k})\bar{q}_{\hat{s}'}(\bar{k}')|(P_0^- + P_{\rm int}^-)$, where $P^- = P_0^- + P_{\rm int}^-$ is the total Hamiltonian of the interacting theory, and $P_{\rm int}$ is given in Eq. (3.9). This gives

$$ \begin{aligned} q^-\,{}_0\langle q_{\hat{s}}(\bar{k})\bar{q}_{\hat{s}'}(\bar{k}')|\gamma^*\rangle &= q^-\cdot 0 + {}_0\langle q_{\hat{s}}(\bar{k})\bar{q}_{\hat{s}'}(\bar{k}')|P_{\rm int}^-|\gamma^*\rangle_0 \\ &\quad + (k^- + k'^-)\delta^3(\bar{q}-\bar{k}-\bar{k}')\psi_{\hat{s}\hat{s}'}(\bar{k}) + \mathcal{O}(e^2), \end{aligned} \tag{3.17} $$

where the term containing $\psi_{ss'}\langle q\bar{q}|P_{\rm int}^-|q\bar{q}\rangle$ is included in $\mathcal{O}(e^2)$ as $\psi_{ss'}\sim e$ and $P_{\rm int}^-\sim e$.

Substituting Eq. (3.16) into (3.17) and relabeling $\hat{s},\hat{s}'\to s,s'$ we find

$$ \delta^3(\bar{q}-\bar{k}-\bar{k}')\psi_{ss'}(\bar{k}) = \frac{{}_0\left\langle q_s(\bar{k})\bar{q}_{s'}(\bar{k}')|P_{\rm int}^-|\gamma^*\right\rangle_0}{q^- - k^- - k'^-}. \tag{3.18} $$

The inner product in Eq. (3.18) can be computed by substituting the Hamiltonian from Eq. (3.9):

$$ \begin{aligned} {}_0\left\langle q_s(\bar{k})\bar{q}_{s'}(\bar{k}')|P_{\rm int}^-|\gamma^*\right\rangle_0 = e_f e \sum_{\hat{s}\hat{s}'\lambda'}\int \mathrm{d}^3\bar{x}\,\text{đ}^3\bar{p}\,\text{đ}\bar{p}'\,\text{đ}^3\bar{l}\,\langle 0|b_s(\bar{k})d_{s'}(\bar{k}') \\ \times\quad [b_{\hat{s}}^\dagger(\bar{p})\bar{u}_{\hat{s}}(\bar{p})e^{ip\cdot x} + d_{\hat{s}}(\bar{p})\bar{v}_{\hat{s}}(\bar{p})e^{-ip\cdot x}] \\ \times\,\gamma^\mu[a^{\lambda'}(\bar{l})\varepsilon_\mu^{\lambda'}(l)e^{-il\cdot x} + a^{\lambda'\,\dagger}(\bar{l})\varepsilon_\mu^{*\,\lambda'}(l)e^{il\cdot x}] \\ \times\quad [b_{\hat{s}'}(\bar{p}')u_{\hat{s}'}(p')e^{-ip'\cdot x} + d_{\hat{s}'}^\dagger(\bar{p}')v_{\hat{s}'}(p')e^{ip'\cdot x}]a^{\lambda\,\dagger}(\bar{q})|0\rangle. \end{aligned} \tag{3.19} $$

Here the factor $(2\pi)^{-3/2}(2p^+)^{-1/2}$ is included in the integration measure đ^3p and e_f is the charge of the quark in terms of the elementary charge (1/3 for d and 2/3 for u quark).

We can then proceed by (anti-)commuting creation and annihilation operators in a term by term basis in such a way that an annihilation operator is moved to the rightmost position or an creation operator is moved to the leftmost position. We use the fact that the annihilation operator destroys the vacuum, and thus $b_p|0\rangle = 0$, and $\langle 0|b_p^\dagger = 0$. As a result the only surviving term from Eq. (3.19) is

$$ \begin{aligned} e_f e \sum_{\hat{s}\hat{s}'\lambda'}\int \mathrm{d}^3\bar{x}\,\text{đ}^3\bar{p}\,\text{đ}^3\bar{p}'\,\text{đ}^3\bar{l}\,\langle 0|b_s(\bar{k})d_{s'}(\bar{k}')b_{\hat{s}}(\bar{p})^\dagger a^{\lambda'}(\bar{l})d(\bar{p}')^\dagger a^\lambda(\bar{q})^\dagger \\ \times\,\bar{u}_{\hat{s}}(p)\not{\varepsilon}^{\lambda'}(l)v_{\hat{s}'}(p')e^{ix(p+p'-q)}\delta_{s\hat{s}}\delta_{s'\hat{s}'}\delta_{\lambda\lambda'}|0\rangle. \end{aligned} \tag{3.20} $$

We continue by using again the (anti-)commutation relations and moving annihilation operators to the rightmost positions. The d^3x integral at $x^+ = 0$ results a factor $(2\pi)^3\delta^3(\bar{p} + \bar{p}' - \bar{q})$. Performing then the momentum integrals and comparing with Eq. (3.18) one gets

$$\psi_{ss'}(k) = e_f e \frac{\bar{u}_s(k)}{\sqrt{(2\pi)^3 2k^+}} \frac{\not{\varepsilon}^\lambda(q)}{\sqrt{(2\pi)^3 2q^+}} \frac{v_{s'}(k')}{\sqrt{(2\pi)^3 2k'^+}} \frac{(2\pi)^3}{q^- - k^- - k'^-}. \tag{3.21}$$

Let us then calculate the required terms. Denoting $Q^2 = -q^2 = -2q^+q^-$ (as $q_T = 0$) and $m^2 = k^2 = 2zq^+k^- - k_T^2$, where m is the quark mass and z is the fraction of light cone momentum carried by the quark ($k^+ = zq^+$), we get

$$\begin{aligned} q^- - k^- - k'^- &= \frac{-Q^2}{2q^+} - \frac{m^2 + k_T^2}{2zq^+} - \frac{m^2 + k_T^2}{2(1-z)q^+} \\ &= -\frac{Q^2 z(1-z) + m^2 + k_T^2}{2q^+ z(1-z)}. \end{aligned} \tag{3.22}$$

The second term we need to calculate is $\bar{u}_s(k)\not{\varepsilon}(q)v_{s'}(k')$. In order to do so we need to specify the polarization vector ε. Considering first a longitudinally polarized virtual photon we can write [10]

$$\varepsilon_L(q) = \left(\frac{q^+}{Q}, 0, \frac{Q}{2q^+}\right) \tag{3.23}$$

in the covariant gauge. Notice that the transverse components are zero. We can then perform a gauge transformation into the light-cone gauge, in which $\varepsilon^+ = 0$:

$$\varepsilon_L(q) \to \varepsilon_L(q) - \frac{q^\mu}{Q} = \left(0, 0, \frac{Q}{2q^+} - \frac{q^-}{Q}\right) = \left(0, 0, \frac{Q}{q^+}\right). \tag{3.24}$$

Now $\not{\varepsilon} = \gamma_-\varepsilon^- = \gamma^+\varepsilon^-$, where the last equality can be seen from $g_{\mu\nu}$, see Eq. (3.2). Thus

$$\bar{u}_s(k)\not{\varepsilon}(q)v_{s'}(k') = \frac{Q}{q^+}\bar{u}_s(k)\gamma^+ v_{s'}(k'). \tag{3.25}$$

Let us then calculate $\bar{u}_s(k)\gamma^+ v_{s'}(k')$. We use the explicit forms for the gamma matrices and Dirac spinors in the chiral basis given in Ref. [12] known

as the Kogut-Soper (KS) convention [11][1]. The spinors are

$$u(k,+1) = \frac{1}{2^{1/4}\sqrt{k^+}} \begin{pmatrix} \sqrt{2}k^+ \\ k_x + ik_y \\ m \\ 0 \end{pmatrix}, \quad u(k,-1) = \frac{1}{2^{1/4}\sqrt{k^+}} \begin{pmatrix} 0 \\ m \\ -k_x + ik_y \\ \sqrt{2}k^+ \end{pmatrix},$$
$$v(k,+1) = \frac{1}{2^{1/4}\sqrt{k^+}} \begin{pmatrix} 0 \\ -m \\ -k_x + ik_y \\ \sqrt{2}k^+ \end{pmatrix}, \quad v(k,-1) = \frac{1}{2^{1/4}\sqrt{k^+}} \begin{pmatrix} \sqrt{2}k^+ \\ k_x + ik_y \\ -m \\ 0 \end{pmatrix}. \tag{3.26}$$

The definitions for the gamma matrices read, in the block diagonal form,

$$\gamma^0 = \begin{pmatrix} 0 & 1 \\ 1 & 0 \end{pmatrix}, \quad \gamma^i = \begin{pmatrix} 0 & -\sigma^i \\ \sigma^i & 0 \end{pmatrix}, \tag{3.27}$$

where σ^i, $i = 1, 2, 3$, are the Pauli spin matrices. Now $\gamma^0\gamma^+ = \sqrt{2}\,\mathrm{diag}(1, 0, 0, 1)$, and clearly

$$u_s^\dagger(k)\gamma^0\gamma^+ v_{s'}(k') = \sqrt{2k^+ 2k'^+}\delta_{s,-s'}. \tag{3.28}$$

Substituting everything back to Eq. (3.21) we get

$$\psi^L_{ss'}(k) = -e_f e \frac{\sqrt{q^+}z(1-z)}{\epsilon^2 + k_T^2} \frac{Q}{q^+} \frac{1}{2\pi\sqrt{\pi}} \delta_{s,-s'}, \tag{3.29}$$

where $\epsilon^2 = Q^2 z(1-z) + m_f^2$ and f is the quark flavor. We then define a new function $\psi^L_{ss'}(z, k_T)$ which is required to satisfy a normalization condition

$$\int \mathrm{d}k^+ |\psi^L_{ss'}(k)|^2 = \int \mathrm{d}z |\psi^L_{ss'}(z, k_T)|^2. \tag{3.30}$$

This requirement is natural as $|\psi|^2$ has an interpretation as a probability of the process $\gamma^* \to q\bar{q}$. As $k^+ = zq^+$, we see that $\psi(z, k_T) = \sqrt{q^+}\psi(k)$.

Finally the result can be Fourier transformed into the transverse coordinate space to get

$$\begin{aligned} \psi^L_{ss'}(z, r_T) &= \frac{-e_f e}{2\pi\sqrt{\pi}} Q z(1-z)\delta_{s,-s'} \int \frac{\mathrm{d}^2 k_T}{2\pi} e^{ik_T \cdot r_T} \frac{1}{\epsilon^2 + k_T^2} \\ &= \frac{-e_f e}{2\pi\sqrt{\pi}} Q z(1-z) K_0(\epsilon r_T)\delta_{s,-s'}. \end{aligned} \tag{3.31}$$

[1]Notice that the expressions for the gamma matrices given in Ref. [11] cannot be used with the KS spinors also quoted in [11], as the sign of γ^i ($i \geq 1$) is different in Refs. [12] and [11].

The final result for the longitudinally polarized virtual photon wave function summed over spins and quark colors is

$$\sum_{s,s',\text{color}} |\psi_L(z,r_T)|^2 = e_f^2 \frac{2N_c\alpha_{\text{em}}}{\pi^2} Q^2 z^2 (1-z)^2 K_0^2(\epsilon r_T), \tag{3.32}$$

where $\alpha_{\text{em}} = e^2/(4\pi)$, and N_c is the number of colors. The function K_0 is the modified Bessel function of the second kind which satisfies $K_0(x) \sim e^{-x}$ at large x, which means that large dipoles are exponentially suppressed. Thus the function $Q^2K_0^2(\epsilon r) \sim Q^2K_0^2(Qr)$ suppresses the processes not satisfying the uncertainty relation $Q \sim 1/r$.

The wave function for a transversely polarized virtual photon can be calculated in a similar manner. The only difference is the polarization vector, which reads, in the light-cone gauge,

$$\varepsilon_T^\lambda(q) = \left(0, \varepsilon_T^\lambda, \frac{q_T \cdot \varepsilon_T^\lambda}{q^+}\right), \tag{3.33}$$

where ε_T^λ are transverse polarization vectors and $\lambda = \pm 1$. The explicit expressions are $\varepsilon_T^1 = (1,i)/\sqrt{2}$ and $\varepsilon_T^{-1} = (1,-i)/\sqrt{2}$ [13]. Notice that in our case the virtual photon has no transverse momentum, and thus $q_T = 0$ and $k_T = -k'_T$.

To compute the wave function we need to calculate the matrix element $\bar{u}_s(k)\varepsilon^\lambda \cdot \gamma_T v_{s'}(k')$. This can be done by using the explicit expressions for the spinors and the gamma matrices, Eqs. (3.26) and (3.27). If $s = s'$, one gets

$$\bar{u}_s(k)\varepsilon_T^\lambda(q) \cdot \gamma_T v_{s'}(k') = \frac{-\lambda - s}{\sqrt{2}} \frac{m_f}{\sqrt{z(1-z)}} \delta_{ss'}. \tag{3.34}$$

Notice that now the matrix element has a dependence on the quark mass m_f which was absent in the longitudinal wave function.

Similarly if $s = -s'$ and $\lambda = +1$ one gets

$$\bar{u}(k)\varepsilon_T^1(q)\gamma_T v_{s'}(k') = -\frac{2}{\sqrt{z(1-z)}} (z\delta_{s,-1}\delta_{s',1} - (1-z)\delta_{s,1}\delta_{s',-1})\, \varepsilon^1 \cdot k_T. \tag{3.35}$$

The matrix element with polarization $\lambda = -1$ can be obtained in a similar manner, and it turns out that the only difference is that one interchanges $s \leftrightarrow s'$. Substituting these matrix elements to Eq. (3.21) we obtain the momentum space wave function

$$\begin{aligned}\psi_{ss'}^{\lambda=\pm1}(k_T) = {} & \frac{e_f e}{\sqrt{(2\pi)^3}\sqrt{q^+}} \frac{1}{\epsilon^2 + k_T^2} \\ & \times \sqrt{2}(z\delta_{s,\mp1}\delta_{s',\pm1} - (1-z)\delta_{s,\pm1}\delta_{s',\mp1})\, \varepsilon^{\pm1} \cdot k_T + m_f \delta_{s,\pm1}\delta_{s',\pm1}\end{aligned} \tag{3.36}$$

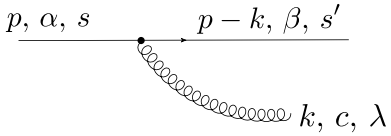

Figure 3.2. Quark with momentum p, spin s and color α emits a gluon with momentum k, color c and polarization λ. The color and spin of the quark after the emission are β and s', respectively.

This can be Fourier transformed into the transverse coordinate space similarly as we did with the longitudinal polarization:

$$\begin{aligned}\psi_{ss'}^{\lambda=\pm1}(z,r_T) &= \int \frac{\mathrm{d}^2k_T}{2\pi} e^{ik_T\cdot r_T}\psi(z,k_T) \\ &= \frac{e_f e}{\sqrt{(2\pi)^3}}\Big[i\sqrt{2}\frac{\varepsilon^{\pm1}\cdot r_T}{|r_T|}K_1(\epsilon r_T)(z\delta_{s,\mp1}-(1-z)\delta_{s,\pm1})\delta_{s,-s'} \\ &\quad + m_f K_0(\epsilon r_T)\delta_{s,\pm1}\delta_{s',\pm1}\Big].\end{aligned} \tag{3.37}$$

Here we used the result $\psi^T(q^+,k_T)=\sqrt{q^+}\psi^T(z,k_T)$ to change a variable to z.

The wave function squared for transversely polarized virtual photons is obtained as an average of the squared wave functions for photons with $\lambda=1$ and $\lambda=-1$. The result reads

$$\sum_{s,s',\mathrm{color}} |\psi_T(z,r_T)|^2 = e_f^2\frac{N_\mathrm{c}\alpha_\mathrm{em}}{2\pi^2}\left\{[z^2+(1-z)^2]\epsilon^2K_1^2(\epsilon r_T)+m_f^2K_0^2(\epsilon r_T)\right\}. \tag{3.38}$$

These functions can be found in the literature, see e.g. Ref. [14]. We also notice that the wave function for longitudinally polarized photon goes to zero in the limit $Q^2\to 0$ whereas the corresponding function for transversally polarized photon does not, which is expected as the real photon can only have a transverse polarization.

3.3 Gluon emission

Let us then study gluon emission from a quark. Our goal is to calculate the amplitude for the process shown in Fig. 3.2, where a quark, with initial momentum p, spin s and color α, emits a gluon with momentum k, color c and helicity λ. The momentum, spin and color of the quark after the emission

are $p-k$, β and s', respectively. We work in the high energy limit, in which p^+ is large and the emitted gluon is soft.

This vertex $q \to qg$ can be calculated in a similar manner as the $\gamma^* \to qq$ amplitude in Sec. 3.2. The result analogous to (3.21) can also be written directly using the Feynman rules of the light-cone QCD perturbation theory which can be found e.g. in Ref. [11]. In our case the relevant rules are

1. For an incoming fermion with momentum p, color α and spin s, add a factor $u_s(p)/\sqrt{(2\pi)^3 2p^+}$.

2. For an outgoing fermion with momentum $p-k$, color β and spin s', add a factor $\bar{u}_{s'}(p-k)/\sqrt{(2\pi)^3 2(p-k)^+}$.

3. To convert incoming lines into outgoing lines, or vice versa, replace $u \leftrightarrow v$, $\bar{u} \leftrightarrow -\bar{v}$ and $\varepsilon \leftrightarrow \varepsilon^*$.

4. For a quark-gluon vertex with quark momentum k, color c and polarization λ, add a factor $g_s t^c_{\alpha\beta} \gamma^\mu \epsilon^\mu_\lambda(k)/\sqrt{(2\pi)^3 2k^+}$, where t^c is the generator of the fundamental representation of SU(3).

5. Multiply the whole expression by a light-cone energy denominator $(2\pi)^3(p^-_{\text{initial}} - p^-_{\text{final}})^{-1} = (2\pi)^3(p^- - k^- - (p-k)^-)^{-1}$.

According to these rules the amplitude for the gluon emission reads

$$\begin{aligned}\Psi_{q\to qg}(k_T, z) = \sqrt{p^+}\frac{\bar{u}(p-k)}{\sqrt{(2\pi)^3 2(p-k)^+}}\frac{t^c_{\alpha\beta} g \not{\epsilon}^\mu_\lambda(k)\gamma_\mu}{\sqrt{(2\pi)^3 2k^+}}\frac{u_s(p)}{\sqrt{(2\pi)^3 2p^+}} \\ \times \frac{(2\pi)^3}{p^- - k^- - (p-k)^-}.\end{aligned} \tag{3.39}$$

Here the prefactor $\sqrt{p^+}$ is added as we have changed the variable to z, the fraction of the quark longitudinal momentum carried by the gluon: $k^+ = zp^+$. In the energy denominator the notation $(p-k)^-$ corresponds to the minus component of the momentum of an on-shell particle having 3-momentum $(\bar{p} - \bar{k})$. In the high-energy limit, where the emitted gluon is soft, we have $z \ll 1$.

We require that the produced gluon is physical (on the mass shell) and thus it can only have transverse polarization. The polarization vector is the same for the gluon as it was for the photon in the previous section, and in $\varepsilon^+ = 0$ gauge it reads

$$\varepsilon^\lambda(k) = \left(0, \varepsilon^\lambda_T, \frac{k_T \cdot \varepsilon^\lambda_T}{k^+}\right). \tag{3.40}$$

As k^+ is small, ε^- dominates and we can approximate $\gamma_\mu \varepsilon^\mu \approx \gamma^+ \varepsilon^-$.

The matrix element $\bar{u}_s(p-k)\gamma^+ u_{s'}(p)$ can be calculated using the explicit spinors and gamma matrices from Eqs. (3.26) and (3.27), and the result is

$$\bar{u}_s(p-k)\gamma^+ u_{s'}(p) = \sqrt{2p^+ 2(p^+ - k^+)}\delta_{s,s'}. \tag{3.41}$$

Moreover we can calculate the energy denominator to be

$$p^- - k^- - (p-k)^- = p^- - \frac{k_T^2}{2k^+} - \frac{(p-k)_T^2}{2(p-k)^+} \approx \frac{-k_T^2}{2k^+}, \tag{3.42}$$

as k^+ is small. Substituting these results back to Eq. (3.39) we get

$$\Psi_{q\to qg}(z, k_T) = -\frac{\sqrt{2}g}{\sqrt{(2\pi)^3}} t^c_{\alpha\beta} \frac{1}{\sqrt{z}} \frac{k_T \cdot \varepsilon_T}{k_T^2} \delta_{s,s'}. \tag{3.43}$$

In the transverse coordinate space this reads

$$\begin{aligned} \Psi_{q\to qg}(z, r_T) &= \int \frac{\mathrm{d}^2 k_T}{\sqrt{(2\pi)^2}} e^{ik_T \cdot r_t} \Psi_{q\to qg}(k_T, z) \\ &= -i\frac{\sqrt{2}g}{\sqrt{(2\pi)^3}} t^c_{\alpha\beta} \frac{1}{\sqrt{z}} \frac{r_T \cdot \varepsilon_T}{r_T^2} \delta_{s,s'}. \end{aligned} \tag{3.44}$$

To get the last equality we used the result for the Fourier transform of a dot product derived in Appendix A.1.

Chapter 4

Balitsky–Kovchegov equation

4.1 Energy dependence of the scattering amplitude

In Sec. 3.2 we calculated the lowest order amplitude for the $\gamma^* \to q\bar{q}$ splitting. If the dipole is boosted to higher rapidity (it is given more energy), there is more phase space available and the quark or the antiquark can emit a gluon as calculated in Sec. 3.3. Gluon emission is a higher order correction ($\sim \alpha_\mathrm{s}\alpha_\mathrm{em}$) to the virtual photon wave function, and we expect to get some insight of the energy dependence of the scattering amplitude by calculating the amplitude for the process $\gamma^* \to q\bar{q}g$. Recall that we want to describe the energy dependence of the scattering process by calculating the energy evolution in the virtual photon wave function. The following discussion follows Ref. [15].

The graphs contributing to the process $\gamma^* \to q\bar{q}g$ are shown in Fig. 4.1. Using the previously derived result for the virtual photon wave function, Eqs. (3.32) and (3.38), and the gluon emission amplitude, Eq. (3.44), we can write the virtual photon wave function now in the leading order in both α_em and α_s:

$$\begin{aligned} |\gamma^*\rangle = |\gamma^*\rangle_0 &+ \frac{1}{\sqrt{N_\mathrm{c}}} \int \mathrm{d}z\, \mathrm{d}^2 r_T\, \psi^{\alpha\bar{\alpha}}_{\gamma^* \to q\bar{q}}(r_T, z) C(r_T) |q_\alpha(x)\bar{q}_{\bar{\alpha}}(y)\rangle_0 \\ &+ \frac{1}{\sqrt{N_\mathrm{c}}} \int \mathrm{d}z\, \mathrm{d}^2 r_T\, \mathrm{d}z'\, \mathrm{d}^2 r'_T \Psi_{\gamma^* \to q\bar{q}g}(r, r', z, z,') |q_\alpha(x) q_{\bar{\alpha}}(y) g_c(z)\rangle_0. \end{aligned} \tag{4.1}$$

Here we added the factors $N_\mathrm{c}^{-1/2}$ in order to keep $\langle\gamma^*|\gamma^*\rangle$ normalized (the inner product contains a sum over all quark colors i, j and gluon color c). Also, we had to add a yet unknown term $C(r_T)$ to the first term in order to

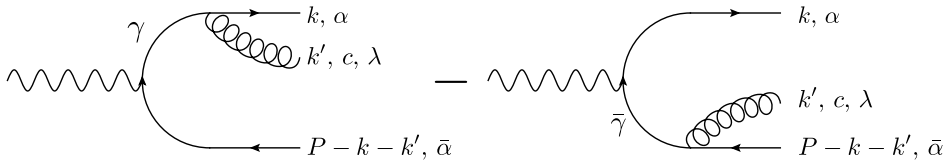

Figure 4.1. Graphs contributing to the process $\gamma^* \to q\bar{q}g$

not alter the normalization of the wave function. We have dropped the spin indices as only one combination of spins survive after the spin summation.

Let us then find the function $\Psi_{\gamma^*\to q\bar{q}g}$. It is straightforward, as we have already calculated the probability amplitude for a quark to emit a gluon, its momentum space expression is given in Eq. (3.43). This allows us to directly write

$$\begin{aligned}\Psi_{\gamma^*\to q\bar{q}g}(k_T, k_T', z, z') = {}& \psi_{\gamma^*\to q\bar{q}}(k_T + k_T', z)\Psi_{q\to qg}(k_T', z') \\ & - \psi_{\gamma^*\to q\bar{q}}(k_T, z)\Psi_{q\to qg}(k_T', z').\end{aligned} \tag{4.2}$$

The relative minus sign follows from the Feynman rules of the light cone perturbation theory, as in the latter case the gluon is emitted from an antiquark and not from a quark, see rule 3 cited on page 18. This can be understood in terms of the color neutrality: at small momentum k_T' the dipole size is much smaller than $\sim 1/k_T'$ and thus it appears as color neutral and cannot emit a gluon. Only at large enough k_T' the gluon can see a localized color charge (quark or antiquark). In order to obtain this property the relative sign between the graphs must be minus.

Using the explicit form of the function $\Psi_{q\to qg}$, Eq. (3.43), we can calculate the Fourier transform of $\Psi_{\gamma^*\to q\bar{q}g}$ into transverse coordinate space:

$$\begin{aligned}\Psi_{\gamma^*\to q\bar{q}g}(r_T, r_T', z, z') = {}& -\int \frac{\mathrm{d}^2k_T'}{\sqrt{(2\pi)^2}} \frac{\mathrm{d}^2k_T}{\sqrt{(2\pi)^2}} e^{ik_T\cdot r_T} e^{ik_T'\cdot r_T'} \frac{g}{\sqrt{4\pi^3 z'}} \frac{\varepsilon_T\cdot k_T'}{k_T'^2} \\ & \times \left[t^c_{\gamma\alpha}\psi^{\bar{\alpha}\gamma}_{\gamma^*\to q\bar{q}}(k+k', z) - t^c_{\bar{\alpha}\bar{\gamma}}\psi^{\bar{\gamma}\alpha}_{\gamma^*\to q\bar{g}}(k, z)\right].\end{aligned} \tag{4.3}$$

Here the superscript $\bar{\gamma}\alpha$ in the function $\psi_{\gamma^*\to qq}$ means that we produce a quark with color α and antiquark with color $\bar{\gamma}$. Summation over repeated color indices is understood, and due to the conservation of color charge $\psi^{\bar{\alpha}\gamma} \sim \delta^{\bar{\alpha}\gamma}$, and thus $t^c_{\gamma\alpha}\psi^{\bar{\alpha}\gamma} \sim t^c_{\bar{\alpha}\alpha}$. Making a change of variables $k \to k - k'$ in the first term and integrating over k_T one gets

$$\begin{aligned}\Psi_{\gamma^*\to q\bar{q}g}(r_T, r_T', z, z') = {}& -\frac{g_s t^c_{\bar{\alpha}\alpha}}{4\pi^2\sqrt{\pi z'}}\psi^{\alpha\bar{\alpha}}_{\gamma^*\to q\bar{q}}(r_T, z) \\ & \times \int \mathrm{d}^2k_T' \left[e^{ik_T'\cdot(r_T'-r_T)} - e^{ik_T'\cdot r_T'}\right] \frac{\varepsilon_T\cdot k_T'}{k_T'^2}.\end{aligned} \tag{4.4}$$

Now it is instructive to notice the geometrical interpretation of r_T'. In the first case, when the gluon is emitted from the quark, the transverse momentum of the gluon, k_T', is the canonical conjugate of $r_T' - r_T$. This suggests that $r_T' - r_T$ is the transverse separation of the quark and the gluon. Similarly when the gluon is emitted from the antiquark, r_T' conjugates with k_T' and thus r_T' is a vector between the positions of the gluon and the antiquark. In both cases r_T is the distance between the quark and the antiquark.

The remaining Fourier transform can be calculated by using the result for the Fourier transform of the dot product, Eq. (A.1), derived in Appendix A.1. The result is

$$\Psi_{\gamma^*\to q\bar{q}g}(r_T, r_T', z, z') = -\frac{ig_s t^c_{\bar{\alpha}\alpha}}{2\pi\sqrt{\pi z'}}\psi^{\alpha\bar{\alpha}}_{\gamma^*\to q\bar{q}}(r_T, z)\left(\frac{\varepsilon_T \cdot r_T'}{r_T'^2} - \frac{\varepsilon_T \cdot (r_T' - r_T)}{(r_T' - r_T)^2}\right). \tag{4.5}$$

Let us then return back to Eq. (4.1) and require that the wave function is still normalized properly. To lowest order, without the gluon radiation term, the inner product is (summation over the quark color indices α and $\bar{\alpha}$ is understood)

$$\langle\gamma^*|\gamma^*\rangle = 1 + \frac{1}{N_\mathrm{c}}\int \mathrm{d}z\,\mathrm{d}^2 r_T |\psi^{\alpha\bar{\alpha}}_{\gamma^*\to q\bar{q}}(r_T, z)|^2 = 1 + \int \mathrm{d}z\,\mathrm{d}^2 r_T |\psi_{\gamma^*\to q\bar{q}}(r_T, z)|^2. \tag{4.6}$$

On the other hand, when the gluon production term is taken into account, the inner product reads

$$\begin{aligned}\langle\gamma^*|\gamma^*\rangle = {} & 1 + \frac{1}{N_\mathrm{c}}\int \mathrm{d}z\,\mathrm{d}^2 r_T |C(r_T)|^2 |\psi^{\alpha\bar{\alpha}}_{\gamma^*\to q\bar{q}}(r_T, z)|^2 \\ & + \int \mathrm{d}z\,\mathrm{d}^2 r_T\,\mathrm{d}z'\mathrm{d}^2 r_T' |\psi_{\gamma^*\to q\bar{q}}(r_T, z)|^2 \frac{g^2}{N_\mathrm{c} 4\pi^3 z'} t^c_{\alpha\bar{\alpha}} t^c_{\bar{\alpha}\alpha} \left|\varepsilon_T^\lambda \cdot \left(\frac{r_T'}{r_T'^2} + \frac{(r_T - r_T')^2}{(r_T - r_T')^2}\right)\right|^2\end{aligned} \tag{4.7}$$

Here we used the fact that the matrices t^c are hermitian: $(t^c_{\alpha\bar{\alpha}})^* = t^c_{\bar{\alpha}\alpha}$. Summation is taken over the transverse polarization states $\lambda = 1, 2$ of the produced gluon and the quark and the gluon color indices α, $\bar{\alpha}$ and c. We can then use the property

$$\sum_{\lambda=1,2} \varepsilon_\lambda^* \cdot x\, \varepsilon_\lambda \cdot x' = x \cdot x'. \tag{4.8}$$

This can be seen from the explicit expressions of the polarization vector quoted in Sec. 3.2. In addition we notice that $t^c_{\bar{\alpha}\alpha} t^c_{\alpha\bar{\alpha}} = (N_\mathrm{c}^2 - 1)/2$. These

results allow us to write Eq. (4.7) as

$$\begin{aligned}\langle\gamma^*|\gamma^*\rangle = 1 + \frac{1}{N_\mathrm{c}}\int \mathrm{d}z\,\mathrm{d}^2 r_T |\psi^{\alpha\bar{\alpha}}_{\gamma^*\to q\bar{q}}(r_T,z)|^2 \\ \times\left[|C(r_T)|^2 N_\mathrm{c} + \int \mathrm{d}^2 r'_T \frac{\mathrm{d}z'}{z'}\frac{g^2}{4\pi^3}\frac{N_\mathrm{c}^2-1}{2}\frac{r_T^2}{r_T'^2(r_T-r'_T)^2}\right].\end{aligned} \tag{4.9}$$

The integral over r'_T is divergent in the limits $r'_T \to 0$ and $r'_T \to r_T$, and we keep the required regulators implicit. We shall see later that these divergences cancel in the BK equation.

Comparing equations (4.6) and (4.9) we see that we must take

$$|C(r_T)|^2 = 1 - \int \mathrm{d}^2 r'_T\,\mathrm{d}y \frac{\alpha_s N_\mathrm{c}}{2\pi^2}\frac{r_T^2}{r_T'^2(r_T-r'_T)^2}, \tag{4.10}$$

where we used the large-N_c approximation $(N_\mathrm{c}^2-1)/N_\mathrm{c} \approx N_\mathrm{c}$ and the fact that the rapidity difference is $y = \ln(1/z')$. We also denoted $\alpha_s = g^2/(4\pi)$.

Let us then use this result to derive an equation for the energy dependence of the forward elastic dipole-target scattering amplitude N, introduced in Eq. (2.7), by boosting the dipole from rapidity y to rapidity $y+\Delta y$. This boost opens a phase space region where a gluon can be emitted, and the probability for the dipole to emit a gluon is

$$\frac{1}{N_\mathrm{c}}\sum_{\text{color}} |\Psi_{q\bar{q}\to q\bar{q}g}(r_T, r'_T, z, z')|^2 \mathrm{d}z'\mathrm{d}r'_T = \frac{\alpha_s N_\mathrm{c}}{2\pi^2 z'}\frac{r_T^2}{r_T'^2(r_T-r'_T)^2}\mathrm{d}z'\mathrm{d}^2 r'_T, \tag{4.11}$$

as the expression for $|\Psi_{q\bar{q}\to q\bar{q}g}|^2$ can be read from Eq. (4.9). The contribution from the $q\bar{q}g$ channel to the forward elastic scattering amplitude is

$$\frac{\alpha_s N_\mathrm{c}}{2\pi^2}\int \mathrm{d}y\,\mathrm{d}^2 r'_T \frac{r_T^2}{r_T'^2(r_T-r'_T)^2} N_{q\bar{q}g}(y, r_T, r'_T), \tag{4.12}$$

where $N_{q\bar{q}g}$ is the forward elastic amplitude for the $q\bar{q}g$ system to scatter off the hadron, and we again wrote $y = \ln(1/z')$. On the other hand the probability to have a $q\bar{q}$ state is reduced by a factor $1-|C(r)|^2$.

We can now write a renormalization group equation for $N_{q\bar{q}}$, the elastic forward amplitude for the dipole to scatter off the target. The emitted gluon can be seen as a part of the virtual photon wave function, in which case our scattering amplitude is

$$N_{q\bar{q}}(y, r_T) + \frac{\alpha_s N_\mathrm{c}}{2\pi^2}\int \mathrm{d}y\,\mathrm{d}^2 r'_T \frac{r_T^2}{r_T'^2(r_T-r'_T)^2}\left[N_{q\bar{q}g}(y, r_T, r'_T) - N_{q\bar{q}}(y, r_T)\right]. \tag{4.13}$$

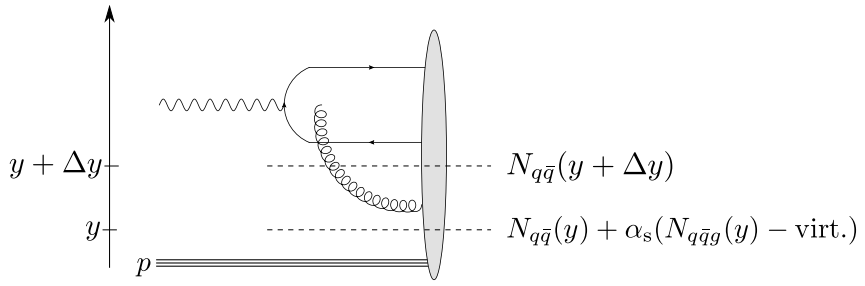

Figure 4.2. The emitted gluon can be seen as a part of the hadron wave function (lower dashed line) or as a part of the dipole wave function (upper dashed line).

This corresponds to the lower dashed line in Fig. 4.2: the dipole-gluon system scatters off the hadron.

On the other hand if the gluon is taken to be a part of the hadron wave function, we have a dipole at rapidity $y + \Delta y$ which scatters off the hadron. This corresponds to the upper dashed line in Fig. 4.2. Physical observables cannot depend on this choice, and we require that the scattering amplitudes obtained in both cases are the same. This gives us a renormalization group equation

$$N_{q\bar{q}}(y + \Delta y, r_T) = N_{q\bar{q}}(y, r_T) + \frac{\alpha_s N_{\mathrm{c}}}{2\pi^2} \Delta y \int \mathrm{d}^2 r'_T \frac{r_T^2}{r_T'^2 (r_T - r'_T)^2} \times \left[N_{q\bar{q}g}(y, r_T, r'_T) - N_{q\bar{q}}(y, r_T) \right]. \tag{4.14}$$

The real contribution contained in term $N_{q\bar{q}g}$ follows from the new process where one gluon is emitted, and the virtual correction $-N_{q\bar{q}}$ is a result of the wave function normalization requirement. Notice that this terminology is a bit different than what is usually used in perturbative QCD calculations: by real contribution we mean a term which is a result of having a new particle in the final state, whereas a virtual contribution follows from the normalization requirement and is proportional to the original amplitude. We have assumed that the rapidity difference Δy is small which allowed us to replace the y integral by a prefactor Δy.

What is still left is to understand the scattering amplitude $N_{q\bar{q}g}$ for a dipole-gluon system to scatter off the hadron. This can be obtained by considering the process in the large-N_{c} limit. The color structure of the emitted gluon is a color-anticolor state, and number of these states is $N_{\mathrm{c}}^2 - 1$ (as the color singlet state is not allowed). At large N_{c}, we have $N_{\mathrm{c}}^2 - 1 \approx N_{\mathrm{c}}^2$, and the gluon can be replaced by two quarks, as the number of different color states for a quark is N_{c}. Thus we assume that the emitted gluon is a new

quark-antiquark pair [16].

Notice that r'_T and $r_T - r'_T$ are distances between the quark/antiquark and the gluon, and now we have effectively two new color dipoles with transverse sizes r'_T and $r_T - r'_T$. The probability for this system to not scatter off the hadron is

$$S_{q\bar{q}g}(r_T, r'_T) = S_{q\bar{q}}(r'_T) S_{q\bar{q}}(r_T - r'_T), \tag{4.15}$$

and keeping in mind that $S = 1 - N$ we get

$$N_{q\bar{q}g}(r_T, r'_T) = N_{q\bar{q}}(r'_T) + N_{q\bar{q}}(r_T - r'_T) - N_{q\bar{q}}(r'_T) N_{q\bar{q}}(r_T - r'_T), \tag{4.16}$$

where the y dependence is kept implicit. Substituting this result back to Eq. (4.14), dividing by Δy and taking the small-Δy limit we get the Balitsky-Kovchegov (BK) equation

$$\begin{aligned} \partial_y N(r_T) = \frac{\bar{\alpha}_s}{2\pi} \int \mathrm{d}^2 r'_T \frac{r_T^2}{r_T'^2 (r_T - r'_T)^2} \\ \times \left[N(r'_T) + N(r_T - r'_T) - N(r_T) - N(r'_T) N(r_T - r'_T) \right], \end{aligned} \tag{4.17}$$

where $\bar{\alpha}_s = \alpha_s N_\mathrm{c}/\pi$, and we dropped the subscript $q\bar{q}$. Notice that the divergences that appeared in Eq. (4.9) cancel when $r'_T \to 0$ and when $r'_T \to r_T$, as $N(r'_T) \to 0$, when $r'_T \to 0$. This equation was first derived by Balitsky in Ref. [17] and by Kovchegov in Ref. [18].

Equation (4.17) is an integro-differential equation and it gives the scattering amplitude $N(r_T)$ at all rapidities $y > 0$ if the initial condition $N(y = 0, r_T)$ is known. We will discuss the initial conditions later in Sec. 4.5. A few words about the interpretation of Eq. (4.17) are, however, in order. The energy evolution follows from the gluon emission which becomes possible when the dipole is boosted to higher rapidity. Integration over the rapidity interval corresponds to multiple gluon emissions and thus we have large number of dipoles in the virtual photon wave function.

The BK equation was derived in the large-N_c limit. If this assumption is not made, one can derive a more general evolution equation known as the JIMWLK (Jalilian–Marian, Iancu, McLerran, Weigert, Leonidov, Kovner) equation. The JIMWLK equation is theoretically and numerically more difficult to study, as it consist of an infinite hierarchy of coupled evolution equations. We do not consider the JIMWLK equation in this work, for a derivation and more detailed analysis see Ref. [1] and references therein.

4.2 The BK equation in momentum space

In previous section we derived the BK equation in coordinate space, where the interpretation is that it gives the energy dependence of the (imaginary

part of the elastic) $q\bar{q}$-hadron scattering amplitude. The interpretation was that as the energy increases, the color dipole is boosted to higher rapidity and it can emit a gluon which can be replaced by a new dipole in a large-N_c limit. In this picture the energy dependence is in the virtual photon wave function, while the target hadron is at rest and does not evolve.

On the other hand we can also view the process in such a frame that the hadron has a large momentum. In this frame the evolution takes place inside the hadron, and the number of small-x gluons in the target hadron increases as a function of energy as we discussed already in Sec. 2.2. The gluon density can be described by an unintegrated gluon distribution function, which can be written as [1]

$$\varphi(k) = \frac{N_c}{4\pi^2\alpha_s}\int \frac{d^2r}{r^2}N(r)e^{ik\cdot r}. \tag{4.18}$$

In order to understand the energy evolution of the unintegrated gluon density we shall study, following e.g. Ref. [19], the quantity

$$N(k) = \int \frac{d^2r}{2\pi r^2}e^{ir\cdot k}N(r), \tag{4.19}$$

which is the same as the unintegrated gluon density up to a constant factor. Following Ref. [19] we identify $N(k)$ as a dipole density in momentum space, or just momentum space dipole amplitude[1]. This transform is called a Fourier transform in some references in this context, even though there is an extra factor r^{-2}.

The gluon distribution function $xg(x,Q^2)$ can then be obtained from the unintegrated gluon distribution by integrating over the transverse momentum [1]. Here we denote the transverse vectors r_T and k_T without the subscript T and use this notation throughout the rest of this work whenever it is clear that we are referring to transverse vectors.

The inverse transform to (4.19) is

$$N(r) = r^2\int \frac{d^2k}{2\pi}e^{-ir\cdot k}N(k). \tag{4.20}$$

The BK equation, Eq. (4.17), can now be transformed into momentum space to obtain the energy dependence of the momentum space dipole amplitude. First we multiply both sides of it by factor

$$\int \frac{d^2(x-y)}{2\pi(x-y)^2}e^{ik\cdot(x-y)}, \tag{4.21}$$

[1]There is also an another way to define unintegrated gluon distribution as a Fourier transform of $S(r) = 1 - N(r)$ (up to a constant) without the extra factor r^{-2}, and it depends on the process which distribution must be used. See discussion in Ref. [20].

where $r = x - y$, $r' = x - z$ and $r - r' = z - y$. As a result we get

$$\partial_y N(k) = \frac{\bar{\alpha}_s}{(2\pi)^2} \int \frac{\mathrm{d}^2 z\, \mathrm{d}^2 (x-y)}{(x-z)^2 (z-y)^2} \times [N(x-z) + N(z-y) - N(x-y) - N(x-z)N(z-y)] e^{ik\cdot(x-y)}. \tag{4.22}$$

We can compute the terms on the r.h.s. of Eq. (4.22) on a term by term basis by using the result

$$i \frac{r}{r^2} \cdot x = \int \frac{\mathrm{d}^2 k}{2\pi} e^{ik\cdot r} \frac{k}{k^2} \cdot x \tag{4.23}$$

for the Fourier transform of the dot product derived in Appendix A.1.

Let us first calculate the contribution from the linear part of the real term on the r.h.s of Eq. (4.22). Writing the coordinate space scattering amplitudes in momentum space using Eq. (4.20) we get

$$\begin{aligned} &\frac{\bar{\alpha}_s}{(2\pi)^2} \int \frac{\mathrm{d}^2 z\, \mathrm{d}^2 (x-y)}{(x-z)^2 (z-y)^2} [N(x-z) + N(z-y)] e^{ik\cdot(x-y)} \\ &= \frac{\bar{\alpha}_s}{(2\pi)^3} \int \mathrm{d}^2 z\, \mathrm{d}^2 (x-y)\, \mathrm{d}^2 q \left[\frac{e^{-iq\cdot(x-z)}}{(z-y)^2} + \frac{e^{-iq\cdot(z-y)}}{(x-z)^2} \right] e^{ik\cdot(x-y)} N(q) \\ &= -\frac{\bar{\alpha}_s}{(2\pi)^5} \int \mathrm{d}^2 z\, \mathrm{d}^2 (x-y)\, \mathrm{d}^2 q\, \mathrm{d}^2 l\, \mathrm{d}^2 l'\, \frac{l\cdot l'}{l^2 l'^2}\, e^{ik\cdot(x-y)} N(q) \\ &\quad \times \left[e^{il\cdot(z-y)} e^{il'\cdot(z-y)} e^{-iq\cdot(x-z)} + e^{il\cdot(x-z)} e^{il'\cdot(x-z)} e^{-iq\cdot(z-y)} \right]. \end{aligned} \tag{4.24}$$

To get the last equality we used Eq. (4.23) to write

$$\frac{1}{(x-z)^2} = \frac{(x-z)\cdot(x-z)}{(x-z)^2 (x-z)^2} = -\int \mathrm{d}^2 l \mathrm{d}^2 l' \frac{l\cdot l'}{l^2 l'^2} e^{il\cdot(x-z)} e^{il'\cdot(x-z)}. \tag{4.25}$$

We then proceed by performing a change of variables $x \to x + y$ and $z \to z + y$ to Eq. (4.24) and integrate over x and z to get

$$-\frac{\bar{\alpha}_s}{2\pi} \int \mathrm{d}^2 q\, \mathrm{d}^2 l\, \mathrm{d}^2 l'\, \frac{l\cdot l'}{l^2 l'^2} N(q) \left[\delta(l + l' + q)\delta(k - q) + \delta(-l - l' - q)\delta(l + l' + k) \right]. \tag{4.26}$$

Integration over q and l' yields

$$\begin{aligned} -\frac{\bar{\alpha}_s}{2\pi} \int \mathrm{d}^2 l \left[\frac{l\cdot(-k-l)}{l^2(-k-l)^2} + \frac{l\cdot(-k-l)}{l^2(-k-l)^2} \right] N(k) \\ = \frac{\bar{\alpha}}{\pi} \int \mathrm{d}^2 l\, \frac{l\cdot(k+l)}{l^2(k+l)^2} N(k). \end{aligned} \tag{4.27}$$

As the scattering amplitude $N(k)$ does not depend on the integration variable l, we notice that the real term in coordinate space gives virtual contribution in momentum space.

The contribution from the virtual term in Eq. (4.22) containing $-N(x-y)$ can be calculated in a similar manner by noticing that $(x-y)^2 = (x-z+z-y)^2 = (x-z)^2 + (z-y)^2 + 2(x-z)\cdot(z-y)$. We get

$$\begin{aligned} &-\frac{\bar{\alpha}_s}{(2\pi)^2}\int \frac{\mathrm{d}^2 z\, \mathrm{d}^2(x-y)}{(x-z)^2(z-y)^2} N(x-y) e^{ik\cdot(x-y)} \\ &= \frac{\bar{\alpha}_s}{(2\pi)^3}\int \mathrm{d}^2 z \mathrm{d}^2(x-y) \mathrm{d}^2 q \frac{(x-z)^2 + (z-y)^2 + 2(x-z)\cdot(z-y)}{(x-z)^2(z-y)^2} \\ &\times e^{-iq\cdot(x-y)} N(q). \end{aligned} \tag{4.28}$$

Using again the identity (4.23) to Fourier transform the dot products into momentum space, performing a change of variables $x \to x+y, z \to z+y$ and integrating over x and z we get

$$\begin{aligned} &-\frac{\bar{\alpha}_s}{2\pi}\int \mathrm{d}^2 q\, \mathrm{d}^2 l\, \mathrm{d}^2 l' \frac{l\cdot l'}{l^2 l'^2} N(q) \\ &\quad\times [\delta(l+l')\delta(k-q) + \delta(-l-l')\delta(l+l'-q+k) + 2\delta(-l+l')\delta(l-q+k)] \\ &= \frac{\bar{\alpha}_s}{\pi}\left[-\int \frac{\mathrm{d}^2 l}{l^2} N(k) + \int \frac{\mathrm{d}^2 q}{(q-k)^2} N(q)\right]. \end{aligned} \tag{4.29}$$

Notice that the virtual term in coordinate space gives both real and virtual terms in momentum space.

Before calculating the contribution from the nonlinear term let us combine the contributions obtained from the real and virtual terms, Eqs. (4.27) and (4.29). The sum of these two terms gives us the BFKL equation [21, 22] which is the same as the BK equation at small densities (small scattering amplitudes), in momentum space. Changing the integration variable to q in all integrals this sum reads

$$\begin{aligned} &\frac{\bar{\alpha}_s}{\pi}\int \mathrm{d}^2 q \left[\frac{q\cdot(k+q)}{q^2(k+q)^2} N(k) - \frac{1}{q^2} N(k) + \frac{1}{(q-k)^2} N(q)\right] \\ &= \frac{\bar{\alpha}_s}{\pi}\int \mathrm{d}^2 q \left[\frac{q\cdot k}{q^2(k+q)^2} N(k) + \frac{1}{(k+q)^2} N(k) - \frac{1}{q^2} N(k) + \frac{1}{(q-k)^2} N(q)\right]. \end{aligned} \tag{4.30}$$

The second and the third term cancel each other.

To proceed we modify the first term in Eq. (4.30) as follows:

$$\begin{aligned}\int \mathrm{d}^2q \frac{q\cdot k}{(q+k)^2q^2} &= \int \mathrm{d}^2q \frac{(q-k)\cdot k}{q^2(q-k)^2} = \int \mathrm{d}^2q \left[\frac{q\cdot k}{q^2(q-k)^2} - \frac{k^2}{q^2(q-k)^2}\right] \\ &= \int \mathrm{d}^2q \left[-\frac{\frac{1}{2}(q-k)^2 - \frac{1}{2}q^2 - \frac{1}{2}k^2}{q^2(q-k)^2} - \frac{k^2}{q^2(q-k)^2}\right] \\ &= -\frac{1}{2}\int \mathrm{d}^2q \frac{k^2}{q^2(q-k)^2}.\end{aligned} \tag{4.31}$$

Substituting this result back to Eq. (4.30) we get the BFKL equation in momentum space:

$$\partial_y N(k) = \frac{\bar{\alpha}_s}{\pi}\int \mathrm{d}^2q \left[\frac{1}{(q-k)^2}N(q) - \frac{1}{2}\frac{k^2}{(q-k)^2q^2}N(k)\right] \tag{4.32}$$

To see that the divergences in Eq. (4.32) cancel let us perform the angular integral using an identity

$$\int_0^{2\pi} \frac{\mathrm{d}\theta}{q^2+k^2-2qk\cos\theta} = \frac{2\pi}{|k^2-q^2|}, \tag{4.33}$$

see Appendix A.2. Integrating Eq. (4.32) over the angular variable we get

$$\partial_y N(k) = \bar{\alpha}_s \int \frac{\mathrm{d}q^2}{q^2}\left[\frac{q^2N(q)-k^2N(k)}{|k^2-q^2|} + \frac{1}{2}\frac{k^2N(k)}{|k^2-q^2|}\right]. \tag{4.34}$$

Finally we use an identity

$$\frac{1}{2}\int \frac{\mathrm{d}q^2}{q^2|k^2-q^2|} = \int \frac{\mathrm{d}q^2}{q^2\sqrt{k^4+4q^4}}, \tag{4.35}$$

derived in Appendix A.2, to get the final form of the BFKL equation in momentum space:

$$\partial_y N(k) = \bar{\alpha}_s \int \frac{\mathrm{d}q^2}{q^2}\left[\frac{q^2N(q)-k^2N(k)}{|k^2-q^2|} + \frac{k^2N(k)}{\sqrt{4q^4+k^4}}\right]. \tag{4.36}$$

This expression is clearly finite when $q \to k$ and when $q \to 0$.

Let us then calculate the contribution from the nonlinear term $\sim N(x-z)N(z-y)$. Using again our definition of the Fourier transform, Eq. (4.19),

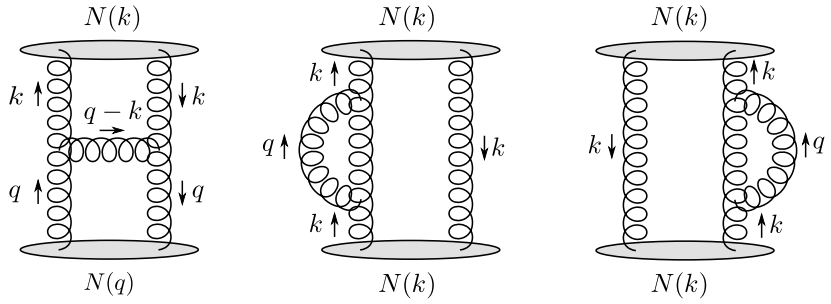

(a) Real gluon emission

(b) Virtual terms

Figure 4.3. Linear contributions to the evolution of the unintegrated gluon distribution in momentum space.

we get

$$\begin{aligned}
&\frac{\bar{\alpha}}{(2\pi)^2}\int \frac{\mathrm{d}^2z\,\mathrm{d}^2(x-y)}{(x-z)^2(z-y)^2}N(x-z)N(z-y)e^{ik\cdot(x-y)}\\
&=\frac{\bar{\alpha}}{(2\pi)^2}\int \frac{\mathrm{d}^2z\,\mathrm{d}^2x\,\mathrm{d}^2q\,\mathrm{d}^2q'}{(x-z)^2(z-y)^2}\\
&\quad\times\frac{(x-z)^2}{2\pi}e^{-iq\cdot(x-z)}N(q)\frac{(z-y)^2}{2\pi}e^{-iq'\cdot(z-y)}N(q')e^{ik\cdot(x-y)}\\
&=\frac{\bar{\alpha}}{(2\pi)^4}\int \mathrm{d}^2z\,\mathrm{d}^2x\,\mathrm{d}^2q\,\mathrm{d}^2q'\,e^{iz\cdot(q-q')}e^{ix\cdot(k-q)}N(q)N(q')\\
&=\bar{\alpha}_s N(k)^2.
\end{aligned} \tag{4.37}$$

To get the second equality we made a change of variables $x \to x+y$, $z \to z+y$. Combining this with the momentum space BFKL equation, Eq. (4.36), we get the BK equation in momentum space

$$\partial_y N(k) = \bar{\alpha}_s \int \frac{\mathrm{d}q^2}{q^2}\left[\frac{q^2N(q)-k^2N(k)}{|k^2-q^2|}+\frac{k^2N(k)}{\sqrt{4q^4+k^4}}\right]-\bar{\alpha}_s N(k)^2. \tag{4.38}$$

Notice that in Eq. (4.38) we have only one integration left to do, which makes the momentum space version of the BK equation easy to study numerically.

Let us try to understand this equation in terms of physical quantities. The gluon momentum k conjugates with $x-y$, and is the transverse momentum of the incoming dipole in coordinate space. On the r.h.s of Eq. (4.38) the terms containing $N(k)$ are virtual corrections and the $N(q)$ term is a real gluon emission. These are shown schematically on Fig. 4.3, see also the discussion in Ref. [19].

The saturation scale Q_s was defined as a scale when nonlinear effects become important. In coordinate space the nonlinear effect is the multiple scattering, where both of the produced dipoles scatter off the hadron. In the hadron side (momentum space) the saturation scale can be seen as a characteristic momentum scale of the probed gluons.

4.3 Running coupling in the BK equation

In Sec. 4.1 the strong coupling constant α_s was assumed to be constant when the BK equation was derived, which makes the BK equation to be leading logarithm approximation for summing powers of $\alpha_s \ln 1/x$ [23]. However the running of the strong coupling, which is a next-to-leading order correction, is known to affect significantly many observables. Thus it is important to study the BK equation with the running coupling as well.

Heuristically one can add the running coupling to the BK equation by replacing $\alpha_s \to \alpha_s(r^2)$ in coordinate space and $\alpha_s \to \alpha_s(k^2)$ in momentum space. Here r and k are the transverse separation and momentum of the parent dipole, respectively. We will refer to this running coupling scheme later in this work as the "parent dipole" prescription and write the kernel in coordinate space as

$$K^{\text{parent}} = \frac{N_c \alpha_s(r^2)}{2\pi^2} \frac{r^2}{r_1^2 r_2^2}, \tag{4.39}$$

where $r_1 = r'$ and $r_2 = r - r'$. Notice that if the parent dipole kernel is used, the results obtained in momentum space transformed to coordinate space are not anymore the same as the results obtained in coordinate space. This is clear from the derivation of the momentum space BK equation performed in Sec. 4.2, as $\bar{\alpha}_s$ was assumed to be $r = x - y$ independent in Eq. (4.22). We will return to this difference later in Sec. 5.2.

The running coupling part of the next-to-leading logarithm (NLL) BK equation is obtained by calculating the contribution from the quark bubbles in the gluon lines to all orders. This calculation has been performed by Balitsky in Ref. [24] and Kovchegov and Weigert in Ref. [25]. We shall not go into the involved details of these calculations here, and we just quote the results.

The running coupling kernel in the Balitsky prescription reads

$$K^{\text{Bal}} = \frac{N_c \alpha_s(r^2)}{2\pi^2} \left[\frac{r^2}{r_1^2 r_2^2} + \frac{1}{r_1^2} \left(\frac{\alpha_s(r_1^2)}{\alpha_s(r_2^2)} - 1 \right) + \frac{1}{r_2^2} \left(\frac{\alpha_s(r_2^2)}{\alpha_s(r_1^2)} - 1 \right) \right]. \tag{4.40}$$

The dominant scale can be seen to be the smallest of r^2, r_1^2 and r_2^2, and thus the coupling has the smallest possible value. We then expect to have a smaller

evolution speed when the Balitsky prescription for the running coupling is used, compared with the parent dipole kernel. Notice that the limit of small r (when $r \ll r_1, r_2$) implies that $K^{\rm Bal} = K^{\rm parent}$.

On the other hand in the Kovchegov-Weigert prescription the kernel is

$$K^{\rm KW} = \frac{N_{\rm c}}{2\pi^2}\left[\frac{\alpha_s(r_1^2)}{r_1^2} - 2\frac{\alpha_s(r_1^2)\alpha_s(r_2^2)}{\alpha_s(R^2)}\frac{r_1\cdot r_2}{r_1^2 r_2^2} + \frac{\alpha_s(r_2^2)}{r_2^2}\right], \tag{4.41}$$

where

$$R^2 = r_1 r_2 \left(\frac{r_2}{r_1}\right)^{\frac{r_1^2+r_2^2}{r_1^2-r_2^2} - 2\frac{r_1^2 r_2^2}{r_1\cdot r_2}\frac{1}{r_1^2-r_2^2}}. \tag{4.42}$$

The apparent disagreement between the prescriptions (4.40) and (4.41) follows from the fact that there is no unique way to include the running coupling correction to the kernel of the BK equation. Instead there is also the so called *subtraction term* which contains the terms not included in the running coupling kernel. It has been shown in Ref. [26] that both Balitsky and KW prescriptions agree when the numerical analysis is performed including the subtraction terms.

The numerical analysis performed in Ref. [26] shows that the Balitsky prescription minimizes the contribution from the subtraction term, and that the subtraction term can be safely neglected at large rapidities. At moderate rapidities, relevant to current experiments, the subtraction term might be numerically important. However, as we will discuss later in Sec. 4.5, one can obtain a good description of the current experimental data even though one neglects the subtraction term.

The strong coupling constant at the given scale r^2 is

$$\alpha_s(r^2) = \frac{12\pi}{(11N_{\rm c} - 2N_{\rm f})\log\left(\frac{4C^2}{r^2\Lambda^2_{\rm QCD}}\right)}. \tag{4.43}$$

$N_{\rm c}$ is the number of colors (3) and $N_{\rm f}$ number of active flavors (3). The dimensionless factor C^2 can be considered as a fit parameter and reflects the uncertainty of the Fourier transform from momentum space, where the running coupling corrections are calculated, to coordinate space [27].

In momentum space we use the expression

$$\alpha_s(k^2) = \frac{12\pi}{(11N_{\rm c} - 2N_{\rm f})\log\left(\frac{C^2k^2}{\Lambda^2_{\rm QCD}}\right)}. \tag{4.44}$$

In momentum space the non-conventional factor C^2, which is different in coordinate and momentum space, is added. We shall see later in Chapter 5

that it is required if we want to get a good description of the experimental data. We follow Ref. [27] and freeze the coupling in both coordinate and momentum space to the fixed value $\alpha_s = 0.7$ in the infrared region in order to avoid divergences.

4.4 Kinematical constraint

In Sec. 4.3 we discussed the running coupling corrections to the BK equation. However, not all next-to-leading logarithm (NLL) corrections can be taken into account by introducing the running coupling. We also noticed that there is no unique way to include running coupling corrections to the BK equation, and we will see later in Chapter 5 that these different prescriptions give significantly different results. Thus it is important to try to understand the complete NLL BK equation.

A full NLL BK equation has been derived in Ref. [28]. Due to the complicated form of that equation it has not yet been studied numerically. Instead, in order to study the importance of the NLL corrections, we consider here, in addition to the running coupling corrections, the so called kinematical constraint.

Let us sketch the derivation of the kinematical constraint to the momentum space BK equation (4.38) following Refs. [29] and [30]. The interpretation of the real term in the BK equation is that we have a splitting $q \to k + k'$ inside the hadron, and as a result a gluon ladder is produced. Part of that ladder is shown in Fig. 4.4. Now in the high energy limit the virtuality of the gluon along the chain must be dominated by the transverse components of the momentum, and the longitudinal momentum factors are strongly ordered: $k^+ \ll q^+$ and $k^- \gg q^-$. This implies that $z = k^+/q^+ \ll 1$. In addition all the transverse momenta are of the same order: $|k_T| \simeq |k'_T| \simeq |q_T|$. If that was not the case, there would be a large suppression $\sim 1/s$ in the gluon propagator [7].

The virtuality of the gluon is

$$k^2 = 2k^+k^- - k_T^2, \tag{4.45}$$

from which we get a requirement

$$k_T^2 > 2|k^+k^-|. \tag{4.46}$$

On the other hand $k^- = q^- - k'^- \approx -k'^-$, as the $-$ component of the momentum increases when we move upwards along the ladder. Using the fact

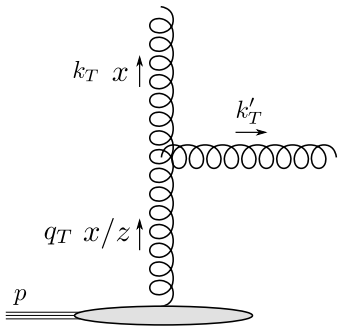

Figure 4.4. Part of the gluon ladder produced by the evolution in rapidity. x and x/z are the longitudinal momentum fractions carried by respective gluons.

that the emitted s channel gluon is on the mass shell we get

$$k^- = -\frac{k_T'^2}{2k'^+} = -\frac{k_T'^2}{2(q^+ - k^+)}. \tag{4.47}$$

Substituting this to Eq. (4.46) we obtain

$$k_T^2 > k_T'^2 \frac{k^+}{q^+ - k^+} = k_T'^2 \frac{z}{1-z} \approx k_T'^2 z. \tag{4.48}$$

This must hold for $k_T'^2 \simeq k_T^2$, which gives just $1 > z$, and for $k_T'^2 \simeq q_T^2$, from which we get the kinematical constraint

$$\frac{q_T^2}{k_T^2} < \frac{1}{z}. \tag{4.49}$$

Noticing that $\ln(1/z)$ is the rapidity difference between the gluons, the constraint can be written as

$$\theta\left(Y - y - \ln\frac{q^2}{k^2}\right), \tag{4.50}$$

where Y and y are the rapidities of the parent and the daughter gluon, respectively. Notice that we again dropped the subscript T as all the vectors from now on in this chapter are transverse. Substituting the constraint directly into the momentum space BK equation to limit the phase space available to the real term we get

$$N(k,Y) = N(k,0) + \bar{\alpha}_s \int_0^Y \mathrm{d}y \int \frac{\mathrm{d}q^2}{k^2} \left[\frac{\theta\left(Y - y - \ln\frac{q^2}{k^2}\right) q^2 N(q,y) - k^2 N(k,y)}{|k^2 - q^2|} + \frac{k^2 N(k,y)}{\sqrt{4q^4 + k^4}} \right] - \bar{\alpha}_s \int_0^Y \mathrm{d}y N^2(k,y). \tag{4.51}$$

To get an integro-differential equation we differentiate both sides w.r.t Y and notice that $\theta'(x) = \delta(x)$. The result is

$$\partial_Y N(k,Y) = \bar{\alpha}_s \int \frac{\mathrm{d}q^2}{q^2} \left[\frac{\theta(k^2-q^2)q^2 N(q,Y) + \theta(q^2-k^2)q^2 N(q^2, Y - \ln\frac{q^2}{k^2})}{|k^2-q^2|} - \frac{k^2 N(k,Y)}{|k^2-q^2|} + \frac{k^2 N(k,Y)}{\sqrt{4q^4+k^4}} \right] - \bar{\alpha}_s N^2(k,Y). \tag{4.52}$$

Notice that Eq. (4.52) is not local in rapidity anymore but it depends on all steps in the evolution. We will study this equation numerically in Sec. 5.4.

For completeness we also mention a few other approaches to include kinematical constraint or energy conservation corrections to the BK equation. In Refs. [31, 32] the authors propose a modified kernel in coordinate space which makes the production of large dipoles exponentially suppressed. In Ref. [33] the kinematical constraint is modeled by requiring that the subsequent gluon emissions are separated by some minimum rapidity interval, which gives a nonlocal BK equation, but the nonlocality does not depend on momentum as it does in Eq. (4.52).

In Ref. [34] a BK equation where the expression for $\partial_y N(r)$ is multiplied by a factor $1-\partial_y$ is derived. This can be interpreted as an energy conservation correction, and it has been studied numerically e.g. in Ref. [35]. A similar energy conservation correction, where the multiplier is $1 - N(r,y)$, is derived in [36]. In this work we do not study these in detail.

4.5 Initial condition and fit to experimental data

The Balitsky-Kovchegov equation, Eq. (4.17), is an integro-differential equation whose solution gives the scattering amplitude at any rapidity $y > 0$ if the inital condition (dipole-hadron scattering amplitude at $y = 0$) is known. This information, however, is of the non-perturbative origin and must be modeled [1].

Many different dipole models have been studied in the literature and compared with the experimental data, see e.g. Refs. [8, 37]. As a result it has been shown that a few different models can describe the current experimental data well. These results justify the use of these dipole models, but the current experimental data is not accurate enough and we cannot say which model is the most realistic one. It has been proposed that the future electron-ion

colliders could be used to study the difference of these dipole models in more detail [38].

The simplest initial condition is the so called Golec-Biernat and Wüsthoff (GBW) dipole cross section introduced first in Ref. [39]. We add an anomalous dimension γ to this model to get what we call a GBW$^\gamma$ model:

$$N^{\mathrm{GBW}^\gamma}(r, y=0) = 1 - \exp\left[-\left(\frac{r^2 Q_{s0}^2}{4}\right)^\gamma\right], \tag{4.53}$$

where the fit parameters are Q_{s0}^2, which is the initial saturation scale squared (recall our discussion about the saturation scale from Sec. 2.2), and the anomalous dimension γ.

The second initial condition is called McLerran-Venugopalan (MV) model derived in Ref. [40]. By including an anomalous dimension we obtain an MV$^\gamma$ model which reads

$$N^{\mathrm{MV}^\gamma}(r, y=0) = 1 - \exp\left[-\left(\frac{r^2 Q_{s0}^2}{4}\right)^\gamma \ln\left(\frac{1}{r\Lambda_{\mathrm{QCD}}} + e\right)\right], \tag{4.54}$$

where again the fit parameters are Q_{s0}^2 and γ. In the original GBW and MV models the anomalous dimension is identically one, $\gamma = 1$. The anomalous dimension mainly affects the shape of the unintegrated gluon density, Eqs. (4.18) and (4.19), at large transverse momentum k. As a consequence, different values for γ cause significantly different transverse momentum distribution in inclusive hadron production in proton-proton and proton-nucleus collisions [41].

The GBW$^\gamma$ and MV$^\gamma$ initial conditions are fitted to the HERA data in Ref. [27], where the authors solved the BK equation using the Balitsky prescription for the running coupling and computed the proton structure function F_2, see Eq. (2.8). The kinematical constraint was not included in the analysis. Even though the subtraction term is neglected in the analysis, the conclusion is that one can obtain a good description of the current experimental data. The values of the fit parameters for the GBW$^\gamma$ and MV$^\gamma$ initial conditions are presented in Table 4.1.

As the impact parameter dependence is neglected in the analysis, σ_0 resulting from the $\int \mathrm{d}^2 b$ integral is also a fit parameter, and it is defined via Eq. (2.7). In Ref. [27] the authors fixed the anomalous dimension γ to be 1 in the GBW$^\gamma$ model as the fits where γ is a free parameter did not show an improvement with respect to those where $\gamma = 1$ was fixed. Thus we use in this work the original GBW model and the MV$^\gamma$ model.

The GBW initial condition is simple enough to be Fourier transformed

Initial condition	σ_0 (mb)	Q_{s0}^2 (GeV^2)	C^2	γ	χ^2/d.o.f.
GBW$^\gamma$	31.59	0.24	5.3	1 (fixed)	1.086
MV$^\gamma$	32.77	0.15	6.5	1.13	1.075

Table 4.1. Values of the free parameters for the GBW$^\gamma$ and MV$^\gamma$ initial conditions obtained in Ref. [27].

into momentum space analytically as we have fixed $\gamma = 1$. The result is

$$N^{\mathrm{GBW}}(k, y=0) = \int \frac{\mathrm{d}^2 r}{2\pi r^2} e^{ik\cdot r} N^{\mathrm{GBW}}(r, y=0) = \frac{1}{2}\Gamma\left(0, \frac{k^2}{Q_{s0}^2}\right). \quad (4.55)$$

Here $\Gamma(0,x)$ is the incomplete gamma function which at large x behaves as $\Gamma(0,x) \sim e^{-x}$. We use this initial condition when we study the BK equation in momentum space.

4.6 Analytical solutions

Let us first study a toy model in $0+1$ dimensions, when the amplitude depends only on the rapidity: $N = N(y)$, and the kernel is simply constant which we denote by $\omega > 0$. Then the BK equation reduces to

$$\partial_y N = \omega(N - N^2). \quad (4.56)$$

This kind of differential equation describes, for example, a self-limiting population growth. The solution of this equation is called a logistic curve and reads

$$N(y) = \frac{e^{\omega y}}{e^{\omega y} + C^{-1}}, \quad (4.57)$$

with initial condition $N(y=0) = C$. We see that for all $C > 0$ the amplitude saturates:

$$N(y) \to 1, \quad \text{when} \quad y \to \infty. \quad (4.58)$$

This toy model teaches us that the fixed point $N = 0$ is unstable and $N = 1$ is stable. If we considered only the linear part of the BK equation (the BFKL equation), there would be an exponential growth in $N(y)$ when y increases.

Let us then study the properties of the linearized BK equation, namely the BFKL equation, in $1+1$ dimension (that is, we neglect the impact parameter dependence). As a starting point we take the BFKL equation in momentum space which we obtain by dropping the nonlinear term from Eq. (4.38):

$$\partial_y N(k) = \bar{\alpha}_s \int \frac{\mathrm{d}q^2}{q^2} \left[\frac{q^2 N(q) - k^2 N(k)}{|k^2 - q^2|} + \frac{k^2 N(k)}{\sqrt{4q^4 + k^4}} \right]. \quad (4.59)$$

The following discussion follows Ref. [7]

Instead of $N(k)$ let us study the function $f(k^2) = k^2 N(k)$. We keep the y dependence of both $N(k)$ and $f(k^2)$ implicit. To solve Eq. (4.59) we first take the Mellin transform of $f(k)$ with respect to k^2:

$$f(\gamma) = \int_1^\infty \mathrm{d}\left(\frac{k^2}{k_0^2}\right)\left(\frac{k^2}{k_0^2}\right)^{-\gamma-1} f(k^2). \tag{4.60}$$

The inverse transform is

$$f(k^2) = \frac{1}{2\pi i}\int_{c-i\infty}^{c+i\infty} \mathrm{d}\gamma \left(\frac{k^2}{k_0^2}\right)^{\gamma} f(\gamma). \tag{4.61}$$

Here k_0 is an arbitrary scale introduced for dimensional reasons and c is a real number. The integral is taken over a straight vertical line in the complex plane.

Replacing $N(k)$ by $f(k^2, y)$ in Eq. (4.59) and substituting Eq. (4.61) into it one obtains

$$\begin{aligned}\frac{1}{2\pi i}\int_{c-i\infty}^{c+i\infty} \mathrm{d}\gamma \left(\frac{k^2}{k_0^2}\right)^{\gamma} \partial_y f(\gamma) = \frac{\bar{\alpha}_s}{2\pi i}\int_{c-i\infty}^{c+i\infty} \mathrm{d}\gamma \int \mathrm{d}q^2 \frac{k^2}{q^2} \\ \times \left\{ \frac{1}{|k^2-q^2|}\left[\left(\frac{q^2}{k_0^2}\right)^{\gamma} - \left(\frac{k^2}{k_0^2}\right)^{\gamma}\right] + \frac{1}{\sqrt{4q^4+k^4}}\left(\frac{k^2}{k_0^2}\right)^{\gamma}\right\} f(\gamma).\end{aligned} \tag{4.62}$$

To proceed we write $(q^2/k_0^2)^\gamma = (k^2/k_0^2)^\gamma (q^2/k^2)^\gamma$ and require that the integrands are equal. Finally we make a change of variables and integrate over $u = q^2/k^2$. After these modifications we obtain

$$\partial_y f(\gamma) = K(\gamma) f(\gamma), \tag{4.63}$$

where the kernel K is given by

$$K(\gamma) = \bar{\alpha}_s \int_0^\infty \frac{\mathrm{d}u}{u}\left[\frac{u^\gamma - 1}{|u-1|} + \frac{1}{\sqrt{4u^2+1}}\right]. \tag{4.64}$$

This is an ordinary differential equation for $f(\gamma, y)$ in rapidity and it is easy to solve:

$$f(\gamma, y) = f(\gamma, y_0) e^{K(\gamma) y}. \tag{4.65}$$

We then want to get the solution in momentum space, which can be obtained by calculating the inverse Mellin transform of $f(\gamma, y)$ by using Eq. (4.61). However let us first study the kernel $K(\gamma)$ in more detail. First we notice that it can be written in terms of the digamma function

$$\psi(x) = \frac{\mathrm{d}\ln\Gamma(x)}{\mathrm{d}x} = \frac{\Gamma'(x)}{\Gamma(x)} \tag{4.66}$$

using the property

$$\psi(s+1) = -\gamma_E + \int_0^1 \mathrm{d}x\, \frac{1-x^s}{1-x} \tag{4.67}$$

valid for $s > 0$. Here $\gamma_E = \psi(0)$ is the Euler-Mascheroni constant $\gamma_E \approx 0.577$. As a result one obtains

$$K(\gamma) = \bar{\alpha}_s \left[2\psi(1) - \psi(\gamma) - \psi(1-\gamma)\right]. \tag{4.68}$$

As $K'(1/2) = 0$ and we want to expand K as a Taylor series, we choose the integration contour in the inverse Mellin transform to be along the line $1/2 + i\nu$ and write

$$\begin{aligned} f(k^2, y) = \frac{1}{2\pi} \int_{-\infty}^{\infty} \mathrm{d}\nu f\left(1/2 + i\nu, y_0\right) \left(\frac{k^2}{k_0^2}\right)^{1/2} \\ \times \exp\left[i\nu \ln\left(\frac{k^2}{k_0^2}\right) + K(1/2+i\nu)\, y\right]. \end{aligned} \tag{4.69}$$

Then we expand $K(1/2 + i\nu) = \lambda - 1/2\lambda'\nu^2 + \mathcal{O}(\nu^4)$, where $\lambda = \bar{\alpha}_s 4 \ln 2$ and $\lambda' = \bar{\alpha}_s 28\zeta(3)$. Here $\zeta(3) \approx 1.202$ is the Riemann zeta function. We also need the expansion of $f(1/2 + i\nu, y_0)$ around $\nu = 0$:

$$\begin{aligned} f(1/2+i\nu, y_0) &\approx f(1/2, y_0) + \nu \left.\frac{\partial f(1/2+i\nu, y_0)}{\partial \nu}\right|_{\nu=0} \\ &= f(1/2, y_0) \left(1 + \nu \left.\frac{\partial \ln f(1/2+i\nu, y_0)}{\partial \nu}\right|_{\nu=0}\right) \\ &\approx f(1/2, y_0) \exp\left(\nu \left.\frac{\partial \ln f(1/2+i\nu, y_0)}{\partial \nu}\right|_{\nu=0}\right) \end{aligned} \tag{4.70}$$

Substituting these expansions back to Eq. (4.69) we get

$$\begin{aligned} f(k^2, y) = \frac{1}{2\pi} \left(\frac{k^2}{k_0^2}\right)^{1/2} f(1/2, y_0)\, e^{\lambda y} \\ \times \int_{-\infty}^{\infty} \mathrm{d}\nu \exp\left[i\nu \ln\left(\frac{k^2}{k_0^2}\right) + \nu \left.\frac{\partial \ln f(1/2+i\nu, y_0)}{\partial \nu}\right|_{\nu=0} - \frac{1}{2}\lambda'\nu^2 y\right]. \end{aligned} \tag{4.71}$$

We can furthermore include the derivative $\partial \ln f / \partial \nu$ into the arbitrary scale k_0^2 by defining

$$\tilde{k}_0^2 = k_0^2 + i \left.\frac{\partial \ln f(1/2+i\nu, y_0)}{\partial \nu}\right|_{\nu=0}. \tag{4.72}$$

After this definition we can and perform the ν integration. Finally we get

$$f(k^2, y) = e^{\lambda y} \left[\frac{k^2/\tilde{k}_0^2}{\pi \lambda' y} \right]^{1/2} \exp\left[-\frac{\ln^2(k^2/\tilde{k}_0^2)}{2\lambda' y} \right], \tag{4.73}$$

or

$$kN(k, y) = \frac{e^{\lambda y}}{\sqrt{\pi \lambda' y}} \exp\left[-\frac{\ln^2(k^2/\tilde{k}_0^2)}{2\lambda' y} \right]. \tag{4.74}$$

A few words about this results are in order. First, the leading energy dependence is $\sim e^{\lambda y}$. In addition the distribution is Gaussian in $\ln k^2$ with a width growing as $\lambda' y$ when y increases. This causes diffusion of the momenta into the ultraviolet and infrared regions. Both of these properties are universal, meaning that they do not depend on the initial condition $f(k^2, y_0)$.

Diffusion into the infrared region causes a potential problem, as even though the evolution was started at hard perturbative scale k_0, the nonperturbative regime $\Lambda_{\rm QCD} \sim k \ll k_0$ is eventually reached. This problem is not present in the solutions to the full BK equation, where the diffusion into the infrared region is strongly suppressed, and the peak of the function $kN(k, y)$ moves toward larger values of k [23].

A completely analogous result can be derived also in coordinate space: dropping the nonlinear term from Eq. (4.17), substituting $U(r) = N(r)/r^2$ and performing the angular integrals one obtains the same equation as Eq. (4.38) (without the nonlinear term) for U [42].

4.7 Impact parameter dependence

The BK equation was derived in Sec. 4.1 by neglecting the impact parameter dependence. As a result the BK equation, Eq. (4.17), is translationally invariant. On the other hand if we consider, for example, electron-nucleus scattering, we expect to have quite strong dependence on the impact parameter (distance between the center of the nucleus and the center of the dipole). For example, the dipole-nucleus scattering amplitude $N(r, b)$ should vanish at large $b \gg R_A$, where R_A is the radius of the nucleus (or proton). The initial condition is chosen in such a way that it satisfies this requirement.

The BK equation with impact parameter dependence has been studied numerically e.g. in Refs. [32, 23], and the corresponding equation in momentum space is derived and studied numerically in Ref. [19]. In coordinate space the

equation reads

$$\partial_y N(b, x_{01}) = \frac{\bar{\alpha}_s}{2\pi} \int \mathrm{d}^2 x_2 \frac{x_{01}^2}{x_{20}^2 x_{12}^2} \left[N\left(b + \frac{x_{12}}{2}, x_{20}\right) + N\left(b - \frac{x_{20}}{2}, x_{12}\right) - N(b, x_{01}) - N\left(b + \frac{x_{12}}{2}, x_{20}\right) N\left(b - \frac{x_{20}}{2}, x_{20}\right) \right]. \tag{4.75}$$

Here $x_{ij} = x_j - x_i$ and b is the impact parameter of the parent dipole. The numerical results obtained in Ref. [23] show that with the impact parameter dependence the scattering amplitude has a very different behavior at large r and constant b: when r increases the amplitude first approaches unity, but then decreases to zero when $r \gg b$. This is a consequence of the fact that in this limit the quarks miss the target but the impact parameter b, which is the average of the positions of the quark and the antiquark, can be small.

When the impact parameter b is large, the amplitude is small and the BK equation reduces to the BFKL equation and causes an exponential growth of the scattering amplitude. This evolution at large b can be interpreted as a growth of the target hadron. This causes the cross section to grow rapidly, as the $\mathrm{d}^2 b$ integral in Eq. (2.7) does not result in a constant factor but increases as a function of rapidity. This growth violates the Froissart bound[2]. Currently there is no consistent way to cut off these long range contributions from the BK equation [23].

As there are still some problems related to the impact-parameter dependent BK equation and as the b-independent equation can be used to describe to experimental data accurately, we did not study the impact parameter dependent equation in this work. The b-independent solutions can be also used to describe, for example, dipole-nucleus scattering if the nucleus is large, as in that case the impact parameter mainly affects the initial saturation scale Q_{s0} which is a free fit parameter in our calculations.

[2]Unitarity in QCD requires that the cross section does not grow faster than $(\ln s)^2$ as a function of invariant energy s. This requirement is called the Froissart bound [43].

Chapter 5

Numerical analysis

5.1 Numerical methods

Let us recall the master results from Chapter 4. The Balitsky-Kovchegov equation was derived in Sec. 4.1, and in transverse coordinate space it reads

$$\partial_y N(r) = \frac{\bar{\alpha}_s}{2\pi} \int \mathrm{d}^2 r' \frac{r^2}{r'^2 (r-r')^2} \left[N(r') + N(r-r') - N(r') - N(r) N(r-r') \right], \tag{5.1}$$

where $N(r)$ is the scattering amplitude and $r = |\bar{r}|$ is the size of the parent dipole. Momentum space version, derived in Sec. 4.2, reads

$$\partial_y N(k) = \bar{\alpha}_s \int \frac{\mathrm{d}q^2}{q^2} \left[\frac{q^2 N(q) - k^2 N(k)}{|k^2 - q^2|} + \frac{k^2 N(k)}{\sqrt{4q^4 + k^4}} \right] - \bar{\alpha}_s N(k)^2. \tag{5.2}$$

Here k is the transverse momentum of the parent dipole, and the transforms between $N(k)$ and $N(r)$ are shown in Eqs. (4.19) and (4.20).

Equations (5.1) and (5.2) are integro-differential equations, but they are numerically straightforward to solve on a lattice. We neglect the impact parameter dependence throughout this work, and thus the amplitude in coordinate space does not depend on angle, $N(\bar{r}) = N(|\bar{r}|)$. This allows us to solve $N(r)$ at discrete values of transverse separation, and we can view Eq. (5.1) as a set of differential equations, where the number of equations equals the number of points on the r grid.

This set of differential equations can then be solved by using standard methods. In order to compute the integral on the r.h.s of Eq. (5.1) using numerical integration routines we interpolate the values of $N(r)$ between the grid points. To be more specific, we use the GNU Scientific Library (GSL) which contains routines for solving the differential equations using the Runge-Kutta method, calculating numerical integrals using adaptive integration

routines and interpolating data points using the cubic spline interpolation. A similar method can be used to solve momentum space version which is numerically less demanding to solve, as the expression for $\partial_y N(k)$ contains only a one-dimensional integral which is easy to compute numerically.

However this straightforward method cannot be used if the kinematical constraint is applied, as one can see from Eq. (4.52), the BK equation in momentum space with kinematical constraint. Equation (4.52) contains a term which is not local in rapidity, and $\partial_Y N(k, Y)$ depends on $N(q, y)$ for all $y < Y$. This makes it impossible to use standard Runge-Kutta methods, and we are forced to use lowest order Euler method to solve this equation numerically. Using small enough step size we have checked that this method gives, within the numerical accuracy, the same results than the Runge-Kutta method if the kinematical constraint is not applied.

In our numerical calculations the initial conditions used in transverse coordinate space are the MV$^\gamma$ model, Eq. (4.54), and the GBW model, Eq. (4.53), with the fit parameters explained in Sec. 4.5. In momentum space we use the GBW model transformed to momentum space, Eq. (4.55). When the kinematical constraint is applied we formally evaluate the amplitude at negative rapidities, and we assume that $N(k, y < 0) = N(k, y = 0)$. Notice that the initial conditions are fit to the experimental data using the Balitsky prescription for the running coupling. We use the same initial conditions also with other running coupling prescriptions in order to see differences between these prescriptions. When comparing with the experimental data the Balitsky prescription must be used.

5.2 Dipole-proton scattering amplitude

We have solved the scattering amplitude $N(r)$ up to asymptotically large rapidities $y = 60$, which corresponds to Bjorken x as small as $x \sim 10^{-30}$. This is far below what can be archived in current and foreseeable future colliders, but is done to understand the asymptotic behavior of the solutions of the BK equation. The result is shown in Fig. 5.1, from which we see that there is little difference between the results obtained using different initial conditions. In addition we notice that the ad-hoc parent dipole kernel gives almost the same results as the KW kernel, but both of these cause much faster evolution than the Balitsky kernel.

In order to study the difference between the two initial conditions and between the running coupling prescriptions in more detail we calculated the

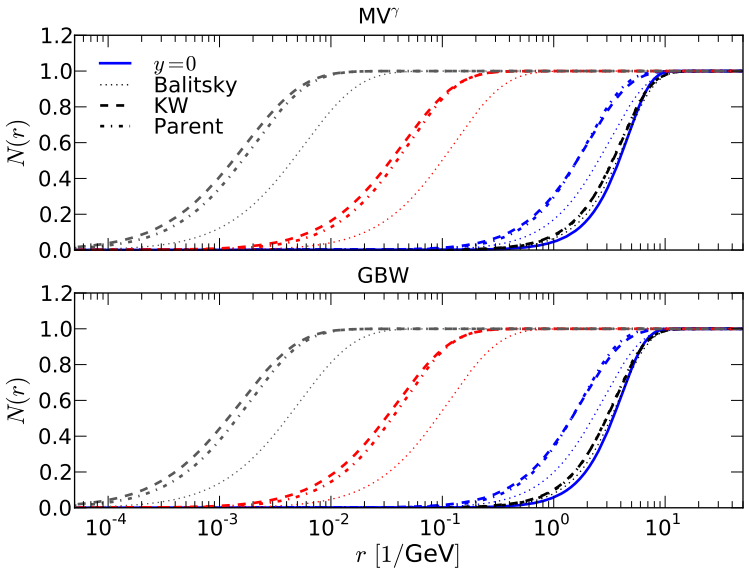

Figure 5.1. Dipole-proton scattering amplitude at rapidities (from right to left) $y = 1$, $y = 5$, $y = 30$ and $y = 60$.

anomalous dimension γ defined as

$$\gamma = \frac{\mathrm{d} \ln N(r)}{\mathrm{d} \ln r^2}. \tag{5.3}$$

Notice that at $y = 0$ and at small r the GBW model, Eq. (4.53), gives $\gamma = 1$ and MV$^\gamma$ model, Eq. (4.54), gives $\gamma = 1.13$. The anomalous dimension is plotted in Fig. 5.2. Even though it behaves differently in MV$^\gamma$ and GBW models, this difference is washed out by the evolution rapidly, and as early as at $y = 5$ the anomalous dimension is basically the same in both cases.

Different evolution speeds can also be seen from Fig. 5.2. As we noticed before, the evolution is much slower when we use the Balitsky prescription. In addition we see that at small r the Balitsky prescription gives the same result as the parent dipole running coupling, which follows from the fact that $K^{\mathrm{Bal}} \approx K^{\mathrm{parent}}$ at small r as discussed in Sec. 4.3. At larger r the parent dipole prescription is closer to the KW kernel. We conclude that the main difference between the Balitsky and the KW prescriptions is that the Balitsky prescription causes slower evolution, but the shape of the solution is the same in both cases. Parent dipole prescription interpolates between these two prescriptions and leads to a slightly different shape for the solution.

In the fixed coupling case ($\bar{\alpha}_s = 0.2$) the solution behaves differently. The anomalous dimension at small r is significantly smaller and this is not just a consequence of the faster evolution speed. As one can see from Fig. 5.2 at

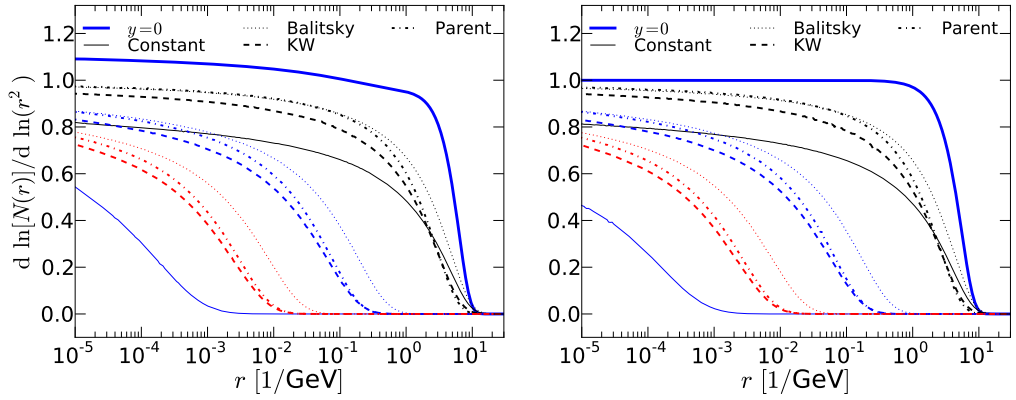

(a) MV$^\gamma$ **(b)** GBW

Figure 5.2. Anomalous dimension γ at rapidities (from right to left) $y = 5$, $y = 30$ and $y = 60$. Constant $\bar{\alpha}_s = 0.2$ is not shown at $y = 60$, as at that point the solution has evolved outside the region shown in the plots.

$y = 5$, the anomalous dimension at large r is actually larger than what is obtained by using the parent dipole or KW prescription.

Let us then study the evolution speed in more detail. Following Ref. [27], we define the saturation scale Q_s trough the condition (compare with Eq. (4.53))

$$N(r = 1/Q_s(y), y) = 1 - e^{-1/4} \approx 0.22. \tag{5.4}$$

As we discussed in Sec. 2.2, Q_s sets the scale at which the nonlinear effects (gluon recombination) become important.

In Sec. 4.6 we saw that the scattering amplitude behaves asymptotically as $\sim e^{\lambda y}$ if the running coupling corrections and nonlinear term are neglected. For the BK equation the saturation scale can be shown to behave approximately as [44]

$$Q_s(y) = Q'_{s_0} e^{v\bar{\alpha}_s y} \tag{5.5}$$

at large y, and $v = 2.44$. As the running coupling corrections slow down the evolution, we expect to get smaller exponent v with the running coupling kernel. Notice that Q'_{s_0} is not the same as the initial saturation scale in the GBW and MV$^\gamma$ models (Eqs. (4.53) and (4.54)).

The numerically solved saturation scale is shown in Fig. 5.3a.The result is as expected, the evolution speed is clearly slower when the running coupling is applied compared with the fixed coupling case. The shape of the function $Q_s(y)$ is also significantly different between the fixed coupling and running coupling solutions. At fixed coupling the solution to the BFKL equation (the BK equation without the nonlinear term) evolves faster than the solution to

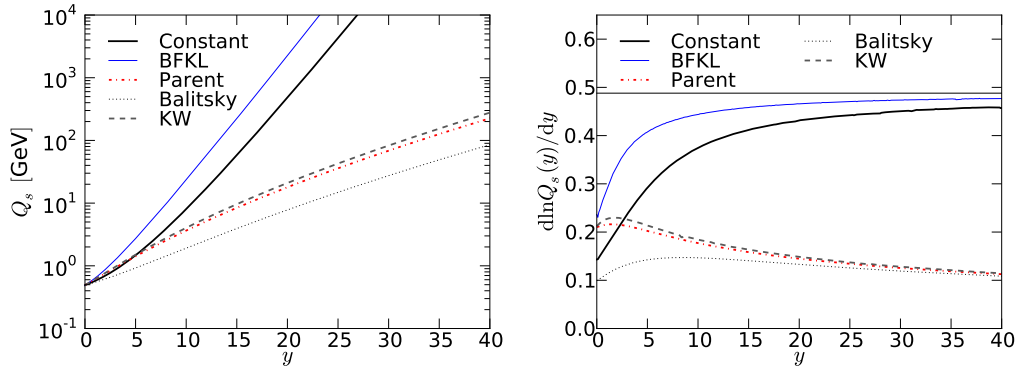

(a) Saturation scale **(b)** Evolution speed

Figure 5.3. The saturation scale in the proton and its logarithmic derivative as a function of rapidity. Initial condition is GBW. The BFKL and fixed coupling BK equations are solved at $\bar{\alpha}_s = 0.2$. The theoretical prediction for the asymptotic value $\mathrm{d}\ln Q_s/\mathrm{d}y = \bar{\alpha}_s v = 0.2 \cdot 2.44$ at large y for the fixed coupling BK equation is also shown.

the fixed coupling BK equation, but the shape of the function $Q_s(y)$ is almost the same in both situations.

The evolution speed can be seen in more detail from Fig. 5.3b, where the logarithmic derivative of the saturation scale (the evolution speed) is shown as a function of rapidity. Our numerical results are consistent with the theoretical prediction $v = 2.44$ at large y. The results suggest that the nonlinear term causes little difference to the evolution speed at large rapidities, as the evolution speeds extracted from the solutions to the fixed coupling BK and BFKL equations are close to each other at large y.

All the running coupling prescriptions can be seen to cause the same evolution speed at large rapidities, and this speed is significantly smaller than what is obtained with fixed coupling. The difference between the running coupling prescriptions is in the evolution speed at moderated rapidities. The parent dipole and KW prescriptions cause almost identical evolution of the saturation scale, whereas the Balitsky prescription yields to much slower evolution.

5.3 Unintegrated gluon distribution

Let us then study the BK equation in momentum space and solve Eq. (5.2) using the initial condition Eq. (4.55), that is, the GBW initial condition transformed to momentum space. The result is the proton unintegrated gluon

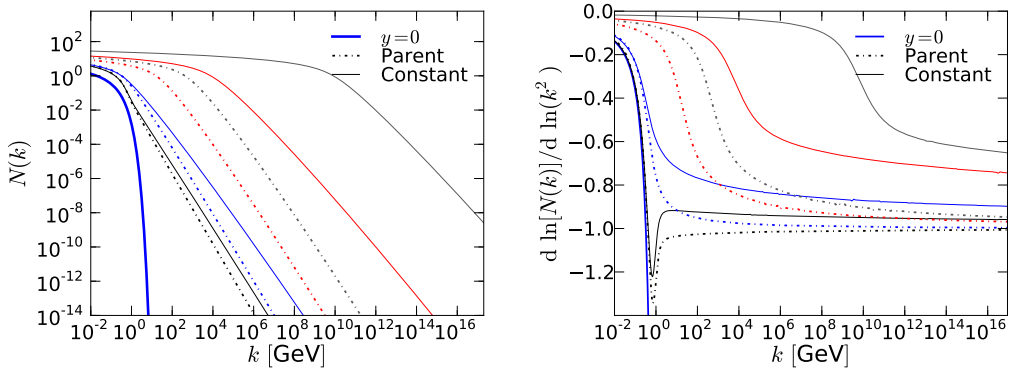

(a) $N(k)$ **(b)** Anomalous dimension

Figure 5.4. Momentum space solution to the BK equation, $N(k)$, and anomalous dimension γ at rapidities (from right to left) $y = 1$, $y = 5$, $y = 30$ and $y = 60$. In the running coupling case the scaling parameter in the expression for α_s is set to $C^2 = 160$.

distribution (up to a constant) as we discussed in Sec. 4.2. The momentum space solution to the BK equation, $N(k)$, is plotted in Fig. 5.4a at various rapidities. We use the parent dipole prescription for the running coupling and compare it with the result obtained by using fixed $\bar{\alpha}_s = 0.2$.

In the running coupling case we set the free parameter $C^2 = 160$ in the expression for α_s, Eq. (4.44). This value is obtained by transforming the solution back to coordinate space and requiring that we obtain the same function as what we would obtain by using the original GBW model and the parent dipole kernel in coordinate space. By setting $C^2 = 6000$ we would get approximately the same result as with the Balitsky running coupling kernel in coordinate space, which we recall to be a fit result describing the currently available experimental data. A comparison of amplitudes from coordinate space and momentum space evolution equations is shown in Fig. 5.5.

The large factor C^2 in the momentum space expression for the running coupling, Eq. (4.44), is somewhat problematic, as it can be interpreted as a scaling of Λ_{QCD} by a large factor C. This factor is required in order to get slow enough evolution speed to reproduce a fit result to the experimental data. An explanation is that the momentum space BK equation with the parent dipole running coupling kernel is not the same as the corresponding equation in coordinate space. This difference comes from the fact that when we transform the BK equation into momentum space, we consider $\bar{\alpha}_s$ as a constant. However with running coupling prescription it depends on the dipole size r, and thus cannot be moved outside the integral in Eq. (4.22) as

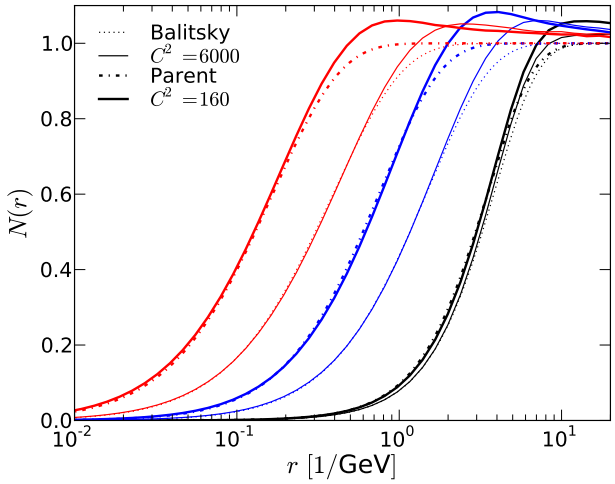

Figure 5.5. Fourier transformed amplitude with parent dipole running coupling and various values of C^2 compared with the solution obtained in coordinate space using the Balitsky and the parent dipole running coupling kernels. Rapidities are from right to left: $y = 1$, $y = 10$ and $y = 20$.

was done in the derivation of the momentum space BK equation in Sec. 4.2. With fixed coupling the equations in momentum and coordinate space are equivalent.

The parent dipole kernel itself is just an ad hoc prescription without any rigorous justification. As the Fourier transform to momentum space is also done by assuming a constant $\alpha_s(r)$, it would be surprising if we actually got the same solution in both coordinate and momentum space. In this context it is interesting to notice that one free scaling parameter in α_s, which slows the evolution, is sufficient to get a good match with the experimental data even when we use an ad hoc type parent dipole kernel.

In addition to the difference in the evolution speed we also notice that if the running coupling is applied, the Fourier transformed amplitude does not respect the unitarity requirement $N \leq 1$. This can be understood, as now we do not have any reason to expect that the momentum space equation with running coupling has the same solution (and same fixed points) as the corresponding coordinate space equation.

In order to study the evolution in more detail we also show the anomalous dimension in momentum space, defined as

$$\gamma = \frac{\mathrm{d} \ln N(k)}{\mathrm{d} \ln k^2}. \tag{5.6}$$

Even though the definition is analogous to the coordinate space definition,

Eq. (5.3), one should notice that the quantities are slightly different. For example, at small k one gets $\gamma \approx -1/(2N(k))$, but in coordinate space the anomalous dimension goes to zero at large r (both of these results follow from the requirement $N(r) \to 1$ at large r).

The anomalous dimension in momentum space is shown in Fig. 5.4b. We can conclude from Figs. 5.4a and 5.4b that the running coupling slows down the evolution significantly. In addition the anomalous dimension at large k is different, which can also be seen directly from Fig. 5.4a: at large k the amplitude falls more steeply when the running coupling is applied. The effect of the running coupling on the anomalous dimension is thus similar than what we observed in coordinate space: running coupling both slows down the evolution and changes the shape of the solution.

5.4 Kinematical constraint

Let us then study the effect of the kinematical constraint discussed in Sec. 4.4. We solved the BK equation applying the kinematical constraint using both the fixed coupling $\bar{\alpha_s} = 0.2$ and the parent dipole running coupling kernels. The numerical solutions are shown in Fig. 5.6. The corresponding anomalous dimensions are shown in Fig. 5.7.

These numerical results suggest that the kinematical constraint affects mainly the evolution speed but not the asymptotic behavior of the solution. The anomalous dimension at large k is the same with and without the kinematical constraint. We conclude that both running coupling and the kinematical constraint make the evolution slower, but their difference is that the running coupling kernel significantly changes the anomalous dimension at large k but the kinematical constraint does not.

The effect caused by the kinematical constraint is numerically more significant if running coupling corrections are not taken into account. With the parent dipole running coupling prescription the effect is still visible even in the log-scale plot, Fig. 5.6b, but significantly smaller.

5.5 Geometric scaling

As we have already noticed, the solutions of the BK equation seem to reach a universal shape independently of the particulars of the initial condition. When this regime is reached, the amplitude is just shifted towards smaller values of the dipole size (larger momentum) when rapidity increases. This property is known as geometrical scaling, which means that the scattering

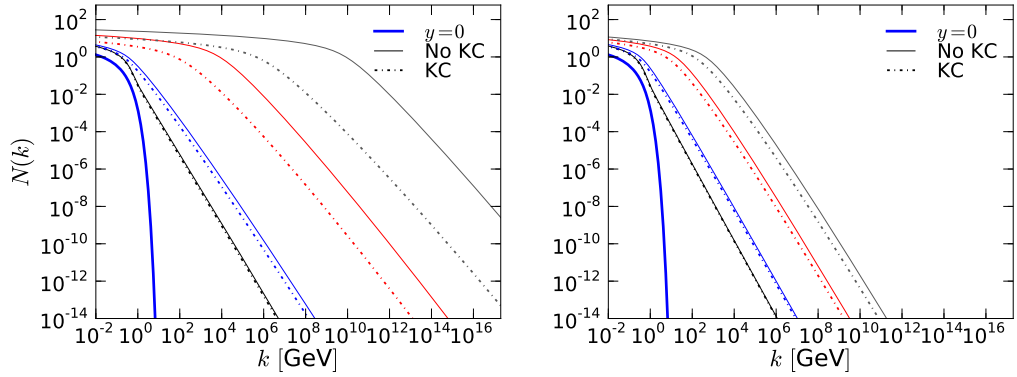

(a) $\bar{\alpha}_s = 0.2$ **(b)** Parent dipole running coupling

Figure 5.6. Scattering amplitude in momentum space at rapidities $y = 1$, $y = 5$, $y = 30$ and $y = 60$ (from left to right) with and without the kinematical constraint (KC). In the running coupling case the scaling parameter in the expression for α_s is set to $C^2 = 160$.

amplitude should only depend on a single dimensionless variable

$$\tau = rQ_s(y) \tag{5.7}$$

instead of r, Q_s and y separately. That is, the only rapidity-dependence is inside the evolution of the saturation scale Q_s. This requirement is natural, as the amplitude is dimensionless and the only relevant dimensionless quantity in the fixed coupling case is rQ_s (Q_s/Λ_{QCD} is an another dimensionless quantity if α_s is not a constant). This property has been observed for example in the HERA data, see e.g. Ref. [45]. Notice that the GBW$^\gamma$ model, Eq. (4.53) satisfies this condition whereas the MV$^\gamma$ model, Eq. (4.54), does not.

Following Ref. [19] we define the saturation scale in momentum space as a maximum of the function $k^{2\gamma_c}N(k)$, where $\gamma_c = 0.5$. The anomalous dimension shown in Fig. 5.4b suggests that the function $N(k)$ decreases as $k^{-2\gamma}$ with $\gamma > 0.5$ at large k, and the exact value of γ depends on the rapidity. The running coupling also increases γ significantly. Thus the interpretation of the saturation scale Q_s is that for $k > Q_s$ the solution has reached a powerlike shape. Using this definition we can also calculate the momentum space solution as a function of the dimensionless variable k/Q_s.

The scattering amplitude in coordinate space as a function of τ is shown in Fig. 5.8, where Q_s is defined via Eq. (5.4). We notice that for the fixed coupling the universal scaling regime is reached at small r as early as $y \lesssim 5$, whereas at larger r we have to evolve up to $y \sim 20$. The asymptotic solution has considerably different shape than the initial condition. This is consistent

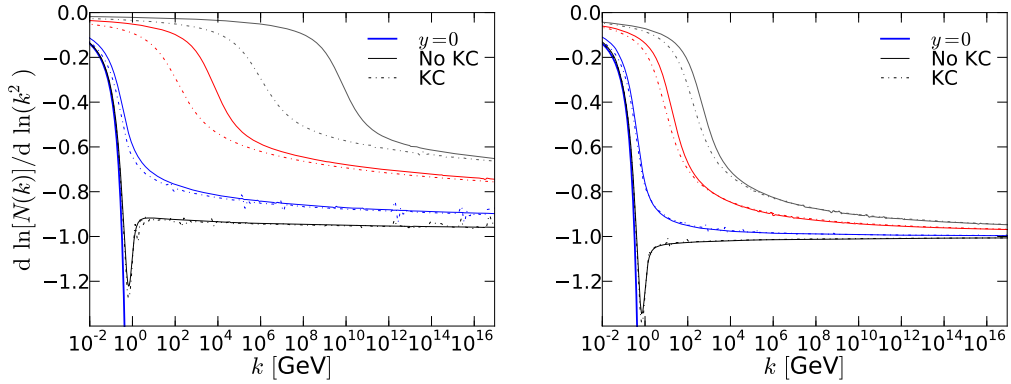

(a) $\bar{\alpha}_s = 0.2$ **(b)** Parent dipole running coupling

Figure 5.7. Anomalous dimension in momentum space at rapidities $y = 1$, $y = 5$, $y = 30$ and $y = 60$ (from left to right) with and without the kinematical constraint (KC). 5.7a: fixed coupling $\bar{\alpha}_s = 0.2$, 5.7b: parent dipole running coupling.

with our results for the anomalous dimension: the initial condition is washed out quickly in the rapidity evolution.

The results obtained with the running coupling seem to have considerably different shape and the shape changes slowly at large rapidities. However it is not clear from our numerical results whether or not the universal shape is eventually reached. As rQ_s is not the only dimensionless scale with the running coupling, we do not have any reason to expect that the geometric scaling also holds if α_s is not constant.

The anomalous dimension in both coordinate and momentum space as a function of dimensionless quantity rQ_s or k/Q_s is shown in Fig. 5.9. In coordinate space the anomalous dimension clearly reaches the asymptotic shape at small rQ_s with fixed coupling, as the anomalous dimension obtained at rapidities $y = 20$ and $y = 40$ are the same within the numerical accuracy. With the running coupling the anomalous dimension at small rQ_s also changes slowly at large y, but it is not clear that it will eventually reach an asymptotic shape.

In momentum space the anomalous dimension at large k/Q_s still changes slightly between rapidities $y = 20$ and $y = 40$ both with and without the running coupling. The evolution slows down when rapidity increases, but we cannot conclude from our results whether or not the anomalous dimension in momentum space will eventually reach an asymptotic shape even with a constant $\bar{\alpha}_s$.

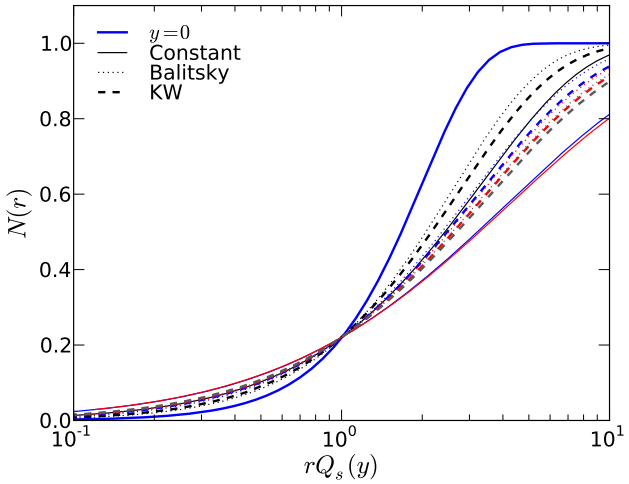

Figure 5.8. Scattering amplitude as a function of $rQ_s(y)$ at rapidities $y = 5$, $y = 20$, $y = 40$ and for running coupling kernels also at $y = 60$ (from up to down at large rQ_s). Initial condition is GBW.

5.6 Structure functions and comparison with the experimental data

In order to check the validity of these calculations we have computed the proton structure function F_2 at small x. This quantity, which is related to the total inelastic electron-proton cross section, is measured within a high accuracy at HERA, see e.g. Refs. [46–48]. It can be computed easily from the dipole-proton scattering amplitude which itself is nothing but our solution to the BK equation, see Eqs. (2.6) and (2.8).

One should keep in mind that this calculation is not a prediction: the free parameters in our initial conditions are fitted to the HERA F_2 data, see discussion in Sec. 4.5. The results are shown in Fig. 5.10. These results are computed using the GBW initial condition and Balitsky prescription for the running coupling which is also used when the initial conditions are fitted to the experimental data, see discussion in Sec. 4.5. The parameters for the GBW initial condition are given in table 4.1.

From Fig. 5.10 we see that theoretical results agree with the experimental data accurately. Thus we conclude that our CGC framework, which in this case consists of the BK equation with the running coupling kernel and lowest order $\gamma^* \to q\bar{q}$ wave function, seems to describe the lepton-hadron scattering at small x very accurately.

In order to test our framework more globally we should calculate also

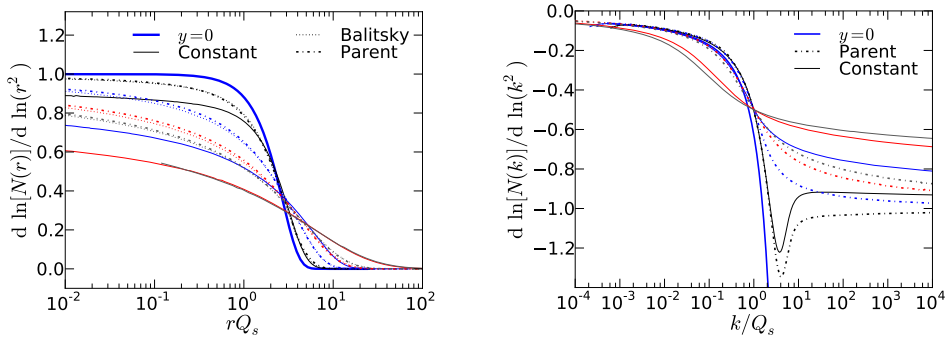

(a) Coordinate space **(b)** Momentum space

Figure 5.9. Anomalous dimension in coordinate and momentum space at rapidities $y = 1$, $y = 5$, $y = 20$ and $y = 40$ from up to down at small rQ_s and from down to up at large k/Q_s or lage rQ_s). The initial condition is GBW.

other observables using the same fit parameters and compare the results with the experimental data. This obviously goes beyond the scope of this work, but for completeness we mention as an example Ref. [49], where the authors calculate hadron spectra in proton-proton collisions using the same fit parameters as we used in this work. Their results are shown to agree with the experimental data from RHIC. It is also shown that one can calculate hadron spectra in deuteron-gold collisions by solving the BK equation for the target nucleus.

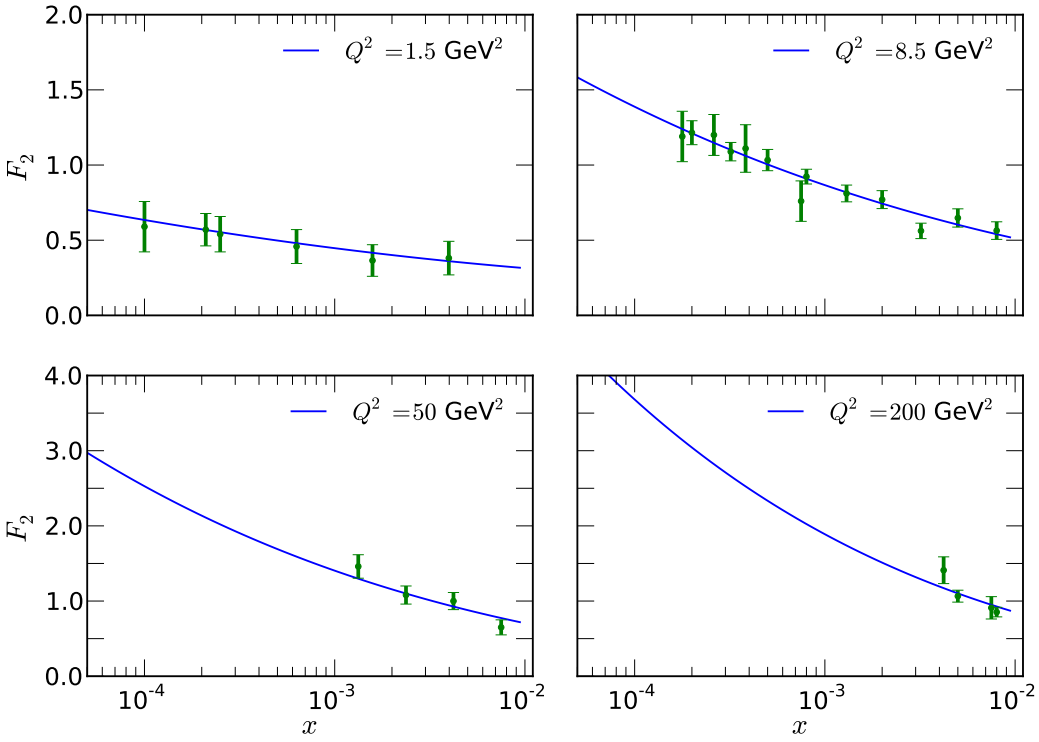

Figure 5.10. Comparison of computed proton structure function F_2 (using the GBW initial condition) with HERA data from Refs. [46–48].

Chapter 6

Conclusions

In this work we derived and studied the Balitsky-Kovchegov (BK) equation, Eq. (4.17). As a solution to this equation we obtained the rapidity (energy) dependence of the dipole-hadron scattering amplitude. We also derived the momentum space BK equation, Eq. (4.38), which gives the rapidity dependence of the unintegrated gluon distribution. In order to derive the BK equation we introduced some concepts of the light cone quantum field theory and used it to calculate amplitudes for processes $\gamma^* \to q\bar{q}$, $q \to qg$ and $\gamma^* \to q\bar{q}g$.

As a part of this work numerical codes for solving the BK equation in both coordinate and momentum space were developed. As the dipole amplitude is an important quantity and appears presently in many calculations in the CGC framework, it is important to have a general-purpose BK code available.

In our numerical studies in coordinate space we noticed that the different running coupling prescriptions to the BK equation yield to significantly different results. The naive way to include the running coupling by replacing α_s by $\alpha_s(r)$ is a good approximation of the Kovchegov-Weigert running coupling, Eq. (4.41). However, both of these prescriptions cause significantly faster evolution than the Balitsky prescription at moderated rapidities, which is argued to be the most accurate running coupling kernel as discussed in Sec. 4.3. At asymptotically large rapidities all the running coupling prescriptions lead to similar evolution speed, and at all rapidities the evolution is significantly slower than what is obtained from solutions with a fixed α_s.

In momentum space we also noticed that the running coupling slows down the evolution. In these calculations we were able to use only the parent dipole kernel for the running coupling, that is, we replaced α_s by $\alpha_s(k)$. In addition we noticed that the asymptotic behavior is changed when the running coupling is applied which is clear from our results for the anomalous dimension: the slope in the $\ln N(k), \ln k$ plane is significantly steeper with

running coupling. The anomalous dimension in coordinate space was also found to behave differently in the fixed coupling and running coupling cases. In order to obtain the same evolution speed in momentum space and in coordinate space, we had to add an arbitrary scaling factor to the definition of $\alpha_s(k)$. Fixing this one scaling parameter appropriately we were able to obtain the same evolution speed in momentum space with parent dipole kernel and in coordinate space with the Balitsky or parent dipole kernels.

In both momentum and coordinate space we saw that the specific form of the initial condition is washed out rapidly. With fixed $\bar{\alpha}_s$ the solution has reached its asymptotic shape at $y \sim 5$, and at large values of y it only travels to smaller values of r (larger values of k). With running coupling it is not clear whether or not an asymptotic shape is eventually reached, at least the shape of the solution still changes slightly around $y \sim 40 - 60$.

The BK equation is derived in a leading logarithm approximation, whereas the running coupling takes into account part of the next to leading logarithm corrections. In order to get some insight of the full next to leading logarithm BK equation we studied the momentum space BK equation with a kinematical constraint, Eq. (4.52). This equation is nonlocal in rapidity which makes numerical calculations more difficult. Our results suggest that the kinematical constraint slows down the evolution significantly in the fixed coupling case, but it is numerically less important if the parent dipole running coupling kernel is used. On the other hand the anomalous dimension (or the shape of the solution) does not change significantly when the kinematical constraint is applied.

Appendix A

Fourier transforms and integrals

A.1 Fourier transform of a dot product

Let us calculate the Fourier transform of a dot product, namely integral

$$\int \mathrm{d}^2k\, e^{ik\cdot r}\frac{k\cdot x}{k^2}, \tag{A.1}$$

where x is an arbitrary 2-dimensional vector. Denoting the angle between k and r by α and between r and x by β we can write Eq. (A.1) as

$$x\int \mathrm{d}k\mathrm{d}\alpha\, e^{ikr\cos\theta}\cos(\alpha+\beta), \tag{A.2}$$

where we denote by x, r and k the lengths of the vectors. Using the trigonometric identity $\cos(\alpha+\beta)=\cos\alpha\cos\beta-\sin\alpha\sin\beta$ we get

$$\begin{aligned}\int \mathrm{d}^2k\, e^{ik\cdot r}\frac{k\cdot x}{k^2} &= x\int \mathrm{d}k\int \mathrm{d}\theta e^{ikr\cos\theta}\left[\cos\alpha\cos\theta-\sin\alpha\sin\theta\right]\\ &= 2\pi i x\cos\alpha\int \mathrm{d}k J_1(kr) = 2\pi i\frac{x}{r}\cos\alpha = 2\pi i\frac{x\cdot r}{r^2},\end{aligned} \tag{A.3}$$

where we used the fact that $J_1'(x)=-J_0(x)$ and noticed that $e^{ikr\cos\theta}\sin\theta$ is proportional to the derivative of $e^{ikr\cos\theta}$ and thus the integral over θ in the second term vanishes.

A.2 Angular integrals

When transforming the BK equation into momentum space on page 30 we used an identity

$$\frac{1}{2}\int \frac{\mathrm{d}q^2}{q^2|k^2-q^2|} = \int \frac{\mathrm{d}q^2}{q^2\sqrt{k^4+4q^4}}. \tag{A.4}$$

This result can be shown as follows. First we notice that making a change of variables $q \to q+k$ we can write

$$\int \frac{\mathrm{d}^2q}{(q-k)^2}\frac{1}{(q-k)^2+q^2} = \int \frac{\mathrm{d}^2q}{q^2}\frac{1}{q^2+(q+k)^2}. \tag{A.5}$$

Let us now calculate the angular integrals over θ, the angle between the vectors k and q, using a standard trigonometric integral

$$\int_0^{2\pi} \frac{\mathrm{d}\theta}{a+b\cos\theta} = \frac{2\pi}{\sqrt{a^2-b^2}}, \tag{A.6}$$

valid for $a+b>0$. From now on we keep the integration limits implicit. The right hand side of Eq. (A.5) directly gives

$$\begin{aligned}\int \frac{\mathrm{d}^2q}{q^2}\frac{1}{q^2+(q+k)^2} &= \int \frac{\mathrm{d}q\, q\,\mathrm{d}\theta}{q^2(2q^2+k^2+2qk\cos\theta)} \\ &= 2\pi\int \frac{\mathrm{d}q\, q}{q^2\sqrt{4q^4+k^4}}.\end{aligned} \tag{A.7}$$

The left hand side of Eq. (A.5) can be computed by noticing that

$$\frac{1}{(q-k)^2+q^2} = \frac{1}{q^2} - \frac{1}{q^2}\frac{(q-k)^2}{q^2+(q-k)^2}. \tag{A.8}$$

After this substitution one can directly use Eq. (A.6) to calculate the angular integrals to obtain

$$\int \frac{\mathrm{d}^2q}{(q-k)^2}\frac{1}{(q-k)^2+q^2} = 2\pi\int \frac{\mathrm{d}q\, q}{q^2\sqrt{(q^2-k^2)^2}} - 2\pi\int \frac{\mathrm{d}q\, q}{q^2\sqrt{4q^4+k^4}}. \tag{A.9}$$

Combining Eqs. (A.9), (A.7) and (A.5), one directly obtains Eq. (A.4).

Bibliography

[1] H. Weigert, *Prog.Part.Nucl.Phys.* **55** (2005) 461 [arXiv:hep-ph/0501087 [hep-ph]].

[2] J. Blaizot, *Nucl.Phys.* **A854** (2011) 237 [arXiv:1101.0260 [hep-ph]].

[3] E. Iancu, A. Leonidov and L. McLerran, arXiv:hep-ph/0202270 [hep-ph].

[4] G. Altarelli and G. Parisi, *Nucl.Phys.* **B126** (1977) 298.

[5] V. Gribov and L. Lipatov, *Sov.J.Nucl.Phys.* **15** (1972) 438.

[6] Y. L. Dokshitzer, *Sov.Phys.JETP* **46** (1977) 641.

[7] E. Predazzi and V. Barone, *High-Energy Particle Diffraction*. Springer, 1 ed., 2002. ISBN 978-3540421078.

[8] H. Kowalski, L. Motyka and G. Watt, *Phys.Rev.* **D74** (2006) 074016 [arXiv:hep-ph/0606272].

[9] H. Mäntysaari, *Nuclear Suppression in Diffractive Vector Meson Production*. University of Jyväskylä, Department of Physics, 2011. Research training report.

[10] F. Halzen and A. D. Martin, *Quarks & Leptons*. Wiley, 1984. ISBN 978-0471887416.

[11] S. J. Brodsky, H.-C. Pauli and S. S. Pinsky, *Phys.Rept.* **301** (1998) 299 [arXiv:hep-ph/9705477].

[12] J. B. Kogut and D. E. Soper, *Phys.Rev.* **D1** (1970) 2901.

[13] M. Peskin and D. Schroeder, *An introduction to quantum field theory*. Advanced book program. Addison-Wesley Pub. Co., 1995. ISBN 978-0201503975.

[14] H. G. Dosch, T. Gousset, G. Kulzinger and H. Pirner, *Phys.Rev.* **D55** (1997) 2602 [arXiv:hep-ph/9608203 [hep-ph]].

[15] T. Lappi, *FYSH560 High energy scattering in QCD*. University of Jyväskylä, Department of Physics, 2011. Lecture notes.

[16] J. Forshaw and D. Ross, *Quantum chromodynamics and the pomeron*. Cambridge lecture notes in physics. Cambridge University Press, 1997. ISBN 978-0521568807.

[17] I. Balitsky, *Nucl.Phys.* **B463** (1996) 99 [arXiv:hep-ph/9509348].

[18] Y. V. Kovchegov, *Phys.Rev.* **D60** (1999) 034008 [arXiv:hep-ph/9901281 [hep-ph]].

[19] C. Marquet and G. Soyez, *Nucl.Phys.* **A760** (2005) 208 [arXiv:hep-ph/0504080 [hep-ph]].

[20] F. Dominguez, C. Marquet, B.-W. Xiao and F. Yuan, *Phys.Rev.* **D83** (2011) 105005 [arXiv:1101.0715 [hep-ph]].

[21] E. Kuraev, L. Lipatov and V. S. Fadin, *Sov.Phys.JETP* **45** (1977) 199.

[22] I. Balitsky and L. Lipatov, *Sov.J.Nucl.Phys.* **28** (1978) 822.

[23] A. M. Stasto, *Acta Phys.Polon.* **B35** (2004) 3069 [arXiv:hep-ph/0412084 [hep-ph]].

[24] I. Balitsky, *Phys.Rev.* **D75** (2007) 014001 [arXiv:hep-ph/0609105 [hep-ph]].

[25] Y. V. Kovchegov and H. Weigert, *Nucl.Phys.* **A784** (2007) 188 [arXiv:hep-ph/0609090 [hep-ph]].

[26] J. L. Albacete and Y. V. Kovchegov, *Phys.Rev.* **D75** (2007) 125021 [arXiv:0704.0612 [hep-ph]].

[27] J. L. Albacete, N. Armesto, J. G. Milhano and C. A. Salgado, *Phys.Rev.* **D80** (2009) 034031 [arXiv:0902.1112 [hep-ph]].

[28] I. Balitsky and G. A. Chirilli, *Phys.Rev.* **D77** (2008) 014019 [arXiv:0710.4330 [hep-ph]].

[29] J. Kwiecinski, A. D. Martin and P. Sutton, *Z.Phys.* **C71** (1996) 585 [arXiv:hep-ph/9602320 [hep-ph]].

[30] K. J. Golec-Biernat, L. Motyka and A. M. Stasto, *Phys.Rev.* **D65** (2002) 074037 [arXiv:hep-ph/0110325].

[31] L. Motyka and A. M. Stasto, *Phys.Rev.* **D79** (2009) 085016 [arXiv:0901.4949 [hep-ph]].

[32] J. Berger and A. Stasto, *Phys.Rev.* **D83** (2011) 034015 [arXiv:1010.0671 [hep-ph]].

[33] G. Chachamis, M. Lublinsky and A. Sabio Vera, *Nucl.Phys.* **A748** (2005) 649 [arXiv:hep-ph/0408333].

[34] A. Kormilitzin and E. Levin, *Nucl.Phys.* **A849** (2011) 98 [arXiv:1009.1468 [hep-ph]].

[35] J. Kuokkanen, K. Rummukainen and H. Weigert, arXiv:1108.1867 [hep-ph].

[36] E. Levin and M. Lublinsky, *Nucl.Phys.* **A730** (2004) 191 [arXiv:hep-ph/0308279].

[37] H. Kowalski and D. Teaney, *Phys.Rev.* **D68** (2003)no. 11 [arXiv:hep-ph/0304189v3].

[38] T. Lappi and H. Mäntysaari, *Phys.Rev.* **C83** (2011) 065202 [arXiv:1011.1988 [hep-ph]].

[39] K. J. Golec-Biernat and M. Wusthoff, *Phys.Rev.* **D59** (1998) 014017 [arXiv:hep-ph/9807513 [hep-ph]].

[40] L. D. McLerran and R. Venugopalan, *Phys.Lett.* **B424** (1998) 15 [arXiv:nucl-th/9705055 [nucl-th]].

[41] A. Dumitru, A. Hayashigaki and J. Jalilian-Marian, *Nucl.Phys.* **A770** (2006) 57 [arXiv:hep-ph/0512129 [hep-ph]].

[42] C. Marquet, *Quantum chromodynamics at high energy, theory and phenomenology at hadron colliders*. 2006. PhD thesis, http://tel.archives-ouvertes.fr/tel-00096416/en/.

[43] M. Froissart, *Phys.Rev.* **123** (1961) 1053.

[44] J. Jalilian-Marian and Y. V. Kovchegov, *Prog.Part.Nucl.Phys.* **56** (2006) 104 [arXiv:hep-ph/0505052].

[45] A. Stasto, K. J. Golec-Biernat and J. Kwiecinski, *Phys.Rev.Lett.* **86** (2001) 596 [arXiv:hep-ph/0007192 [hep-ph]].

[46] **H1** collaboration, S. Aid *et. al.*, *Nucl.Phys.* **B470** (1996) 3 [arXiv:hep-ex/9603004 [hep-ex]].

[47] **H1** collaboration, T. Ahmed *et. al.*, *Nucl.Phys.* **B439** (1995) 471 [arXiv:hep-ex/9503001 [hep-ex]].

[48] **ZEUS** collaboration, M. Derrick *et. al.*, *Z.Phys.* **C69** (1996) 607 [arXiv:hep-ex/9510009 [hep-ex]].

[49] J. L. Albacete and C. Marquet, *Phys.Lett.* **B687** (2010) 174 [arXiv:1001.1378 [hep-ph]].